# General Disclaimer

One or more of the Following Statements may affect this Document

- This document has been reproduced from the best copy furnished by the organizational source. It is being released in the interest of making available as much information as possible.

- This document may contain data, which exceeds the sheet parameters. It was furnished in this condition by the organizational source and is the best copy available.

- This document may contain tone-on-tone or color graphs, charts and/or pictures, which have been reproduced in black and white.

- This document is paginated as submitted by the original source.

- Portions of this document are not fully legible due to the historical nature of some of the material. However, it is the best reproduction available from the original submission.

DRA
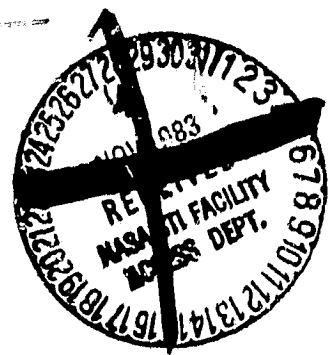
The Pennsylvania State University

The Graduate School

Department of Astronomy

International Ultraviolet Explorer Observations of Wolf-Rayet Binaries:

Wind Structures

A Thesis in

Astronomy

by

Gloria Koenigsberger

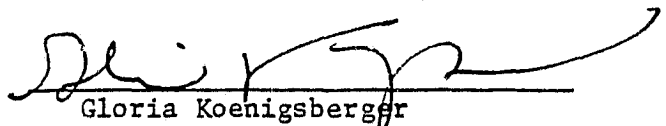Submitted in Partial Fulfillment
of the Requirements
for the Degree of

Doctor of Philosophy

August 1983

We approve the thesis of Gloria Koenigsberger

Date of Signature:

24 June 1983   *Lawrence Auer*

Lawrence H. Auer, Associate
Professor of Astronomy, Thesis Adviser

10 July 1983   *Gordon P. Garmire*

Gordon P. Garmire, Professor of
Astronomy, Chairman of Committee

July 7, 1983   *Satoshi Matsushima*

Satoshi Matsushima, Professor of
Astronomy, Head of the Department of
Astronomy

24 June 1983   *Don N. Page*

Don N. Page, Assistant Professor of
Physics

7 July 1983   *Lawrence W. Ramsey*

Lawrence W. Ramsey, Associate
Professor of Astronomy

7 July 1983   *Daniel W. Weedman*

Daniel W. Weedman, Professor of
Astronomy

ABSTRACT

Spectra of six WN + OB Wolf-Rayet systems obtained with the IUE are analyzed for phase-dependent variations. Periodic variability at emission-line frequencies is detected in V444 Cyg, HD 90657, HD 211853, HD 186943 and HD 94546 on low dispersion SWP ($\lambda\lambda$ 1200 - 1900 A) images. No changes in the low dispersion spectra of HD 193077 are apparent.

We find the variations in the UV to be similar in nature to those observed in optical spectra of various WR sources. That is, there is a strengthening of absorption components in P Cygni - type features at orbital phases in which the O-star is behind the WR wind. With the aid of a computer code which models this type of variations, and through a comparison with HD 193077, the dominant mechanism producing the variations is shown to be selective atmospheric eclipses of the O-star by the WR wind. Based on this interpretation, a straightforward technique is applied to the line of N IV 1718, by which an optical depth distribution in the WN winds of the form $\tau \propto r^{-1}$ is derived for 16 < r < 66 $R_{\odot}$.

The presence of the N IV ionization stage out to at least 66 $R_{\odot}$ is consistent with the proposed constant ionization structure in WN winds (Willis, 1982).

Phase-dependent variations in the width of the C IV 1550 absorption component in V444 Cyg, HD 90657 and HD 211853 are interpretated as wind-wind collision effects.

TABLE OF CONTENTS

LIST OF TABLES

LIST OF FIGURES

ACKNOWLEDGEMENTS

This thesis represents the final stage of my formal academic instruction. Many persons have played important roles throughout this formative period by introducing concepts, influencing philosophical perceptions, and providing valuable instruction. Their guidance, interest and support have made this thesis possible.

In a chronological order, I must first thank Franz Koenigsberger who sparked in me the curiosity and interest in celestrial bodies and in natural phenomena, and Linnea Horowitz who set the stage for my first years of formal education. To both my parents, I express my graditude.

I am deeply indebted to Anthoni Aveni, whose advice and encouragement may be the single most important influence responsible for my career in Astronomy. I sincerely thank him for his continuing interest in my progress during the past eighteen years.

I am profoundly grateful to Manuel Peimbert for the valuable guidance and support he has always given me.

Claudio Firmani introduced me to astronomical research, and is responsible for the framework within which most of my research has been set. I gratefully acknowledge his influence on my work.

Roberto Avena's persistance, confidence and backing are largely responsible for my graduate degree. His support has also enabled me

Chapter I

INTRODUCTION

Since their discovery in 1867 by C. J. E. Wolf and G. Rayet,
the Wolf-Rayet (WR) stars have remained as one of the most interesting
groups of stellar objects. Although considerable theoretical and
observational work has been dedicated to them, and although advances
have been made in determining their properties, an understanding of
these objects has not been achieved.

For the more recent descriptions of their properties and
theoretical advances the reader is referred to the four symposia
and colloquia dedicated to WR stars and related objects (Gebbie and
Thomas, 1968; Bappu and Sahade 1973; Conti and de Loore 1980;
de Loore and Willis 1982), and references cited therein. We will
summarize only the characteristics of WR stars needed to set the
framework within which the present investigation is contained.

The spectra of WR stars are characterized by broad and
intense emission lines. On the basis of these emissions lines,
two general categories or subtypes have been established: The WN's
which show mainly lines of nitrogen and the WC's where carbon and
oxygen lines prevail. In both cases, helium lines are present,
and hydrogen lines are weak or absent. Both categories are
subdivided according to degree of ionization. The WN's are
classified according to decreasing degree of ionization from WN2

to WN10. Analogously, WC's are classified from WC5 to WC9. In most cases, for a given star, a large range in ionization and excitation conditions are represented, the most extreme case having four stages of ionization of the same element visible in its spectrum (Massey and Conti 1980).

Many of the emission lines exhibit P Cygni type profiles. That is, the emission is accompanied by a shortward-shifted absorption component, which is characteristic of envelopes or winds in expansion with respect to a continuum source. It is the presence of these absorptions and the large widths of the emission lines that prompted Beals (1939) to first suggest the existence of massive outflows of material from WR stars. The emission line widths are generally of the order of 3000 km s^{-1}, indicating outflow velocities of at least 1500 km s^{-1}.

Two fundamental problems concerning WR stars are still unsolved: Their evolutionary status and the mechanisms powering the enormeous mass-loss rates observed. Although WR stars are generally considered to be in the late stages of the evolution of massive stars (i.e., post Main Sequence), the conditions necessary for the progenitor to evolve into a WR are unclear. Abundance analyses indicate that WR's have nuclear processed material at their surfaces, with WN subtypes corresponding to stars in which the products of the CNO cycle are on the surface (and hence in

the wind) and WC's showing products of helium burning (Willis
and Wilson 1978; Paczynski 1973). Only for the most massive
stars are mass-loss rates through stellar wind sufficient to
strip away enough layers to uncover nuclear processed material.
In the remaining cases, mass-loss through Roche Lobe overflow in
binary systems, extensive mass-loss during the red supergiant stages,
or some other means of mass-loss is necessary.

Considerable work has been dedicated to the construction
of evolutionary models leading to WR stars. These include the
effects of mass-loss during the Main Sequence, binary membership,
rotation, Roche Lobe overflow, and combinations of these. The
reader is referred to the numerous publications cited in the
reviews by Chiosi (1982) and de Loore (1982).

In addition to the mass-loss necessary to generate a WR star
from a massive progenitor, the WR's are currently in a phase of
moss-loss via a stellar wind. The mass-loss rates which have been
deduced are $\dot{M} \geq 10^{-5}$ $M_\bullet$ yr^{-1}, and are apparently independent of
subtypes and stellar parameters (Barlow, Smith and Willis 1981).
The mechanisms responsible for this large rate are not fully
understood. Apparently, radiation pressure can only account for
part of the mass outflow (Abbott 1982). Thus, other mechanisms
have been invoked in which mechanical energy is generated and then
transmitted to the wind, powering the flow. For example, the

presence of a hot and thin corona just above the photosphere has been proposed (Thomas 1973; Hearn 1975; Cassinelli, Olson and Stalio 1978). Other models include a two-component gas, in which a population of radiatively-driven condensations plough through and are confined by ram pressure of, an ambient non-radiatively driven gas (Lucy and White 1981; Lucy 1982). Finally, Sreenivasan and Wilson (1982) have proposed a model in which a WR star can be viewed as a rapidly rotating core which is being slowed down by the extended envelope with which it is not in co-rotation. The shear energy is then transported to the wind and provides mechanical heating.

Clearly, an understanding of the structure of WR winds can provide an insight into the driving mechanisms. By wind structure, one means the functional dependence of the velocity, density and temperature on position throughout the wind. Due to conservation of mass flow, the density and velocity at each point in the wind may be related ($\dot{M} \propto r^2 v(r) \rho(r)$), and thus if the velocity distribution can be determined, the density distribution follows, and vice-versa.

Several attempts have been made to derive the structure in WR winds by modeling the infrared continous energy distribution assuming free-free emission (Hartmann and Cassinelli 1977; van der Hucht 1979; Hartmann 1978). These resulted in density distributions

corresponding to a wind with an extended constant velocity distribution. Consistent with these results is the analysis of continuum eclipses of V444 Cyg, a well-known WN + OB binary system, where a constant velocity flow is inferred for radial distances $r > 12 R_\odot$ (Cherepashchuk, Eaton and Khaliullin 1981). If this result is correct, then the wind must undergo the initial acceleration close to the continuum-emitting core, but there is no information regarding this region.

Perhaps the only means of determining wind structure is through the analysis of emission line profiles. The basic picture of a WR star consists of a hot continuum-emitting stellar core surrounded by a spherical, rapidly expanding extended atmosphere, in which the emission spectrum is assumed to originate.

The treatment of the radiative transfer in moving atmospheres has been given by Sobolev (1958, 1960) and extended by Castor (1970a). Sobolev was the first to recognize that the presence of a velocity gradient in the extended envelopes of stars such as WR's actually simplifies the line transfer problems for it dominates the photon escape and thermalization process, and implies a geometric localization of the source function. That is, in a rapidly moving extended atmosphere with an expansion velocity far in excess of the thermal velocity, radiative interaction in the lines with distant parts of the atmosphere is negligible

and thus the line transfer is locally constrained. Hence, a line photon emitted in a certain direction at a given frequency in a certain place in the wind is either absorbed immediately, or escapes, and its frequency corresponds to the line-of-sight velocity of the emitting material. The geometrical region from which the emission at any one frequency arises is a surface of constant radial velocity. These surfaces extend over large regions, and their shape depends upon the nature of the velocity field. Thus, we can not associate a given frequency in the line profile with a specific position in the wind, but only with a line-of-sight velocity. Insofar as large regions of the wind may have the same line-of-sight velocity, the wind structure cannot be extracted directly from the observed profiles. The technique usually employed is to model the profiles, using the Sobolev Theory, and to apply different source functions and optical depth distributions. However, this leads to ambiguous results, since line profiles can be reproduced with a variety of dissimilar combinations of optical depth and source functions (Castor 1970a). Thus, as stated by Mihalas (1978, p. 568), a thorough analysis of the spectroscopic data, with the goal of diagnosing physical conditions in the flow semiempirically is necessary and might prove to be very rewarding.

Up to now, all the attempts to model profiles in WR stars have been concentrated to fitting profiles observed in single stars;

i.e., those not associated with OB companions. It has long been known (c. f. Wilson 1940) that line profiles in WR binary systems undergo periodic, phase-dependent variations. Hence, the interaction effects suggested by these variations represent an added complication to an already difficult problem, especially since the mechanism responsible for the variations are not fully understood. However, binary systems can provide an extremely valuable quantity: the scale length within the wind. That is, the orbital separation, which is presumably known in the well studied systems, can be used as a yardstick to establish the geometrical location of emitting and absorbing material within the wind. Specifically, thirty-three years ago Münch (1950) proposed that the eclipses of the OB component by the WR wind are largely responsible for variable P Cygni-type profiles observed in these binary systems. Recent observations at ultraviolet (Willis et al. 1979; Eaton, Cherepashchuk, and Khaliullin 1982) as well as optical (Cowley et al. 1971; Massey and Niemela 1980) frequencies seem to indicate that selective atmospheric eclipses are indeed the dominant mechanism. If this is the case, then the OB component in WR binary systems can be used as a probe of the wind opacity distribution, and hence restrict the number of free parameters in model profile computations.

In this thesis we will investigate the possibility of using phase-dependent profile variations in WR + OB binaries in order to

derive the wind structure of WR stars. We will show that the major profile variability results from selective atmospheric eclipses, and we will empirically derive a first order optical depth distribution for the WR winds.

Chapter II

IUE OBSERVATIONS AND INTREPRETATIONS

Introduction

The ultraviolet (UV) spectral region of WR stars has been
extensively observed since the advent of UV astronomy. References
to the early results are listed by Johnson (1978), while subsequent
observations are reported by Willis and Wilson (1978) and van der
Hucht (1978). However, until the launch of the International
Ultraviolet Explorer (IUE), UV observations of WR stars were
limited to the brightest objects, and to low resolution spectroscopy.

The IUE was launched in early 1978, becoming the first astronomical
satellite to be placed in a geosynchronous orbit, permitting a
greater accessibility of targets. It carries two UV echelle
spectrographs covering the wavelength region 1150 - 1950 Å and
1900 - 3200 Å, respectively, permitting the acquisition of high
resolution (0.1 - 0.2 Å) UV spectra for the first time. Low
resolution (~6 Å) spectra can also be obtained of much fainter
objects than previously possible. The description and performance
of the IUE have been summarized by Boggess (1978, 1979).

The first year of IUE observations of WR stars has been
summarized by Nussbaumer et al. (1979), and subsequent observations
are reported in two volumes published by NASA (Chapman 1981; Kondo,
Mead and Chapman 1982).

The data obtained from ground-based observations suffer from a fundamental limitation: all of the lines observed are subordinate transitions that arise from levels with high excitation potentials, and hence with small populations outside the regions of high temperature and density. The column density of absorbers in these lines is therefore quite small, and one observes only the innermost layers of the wind, just outside the photosphere. In contrast, the UV spectral region contains resonance lines arising from the ground states of the dominant ionization stages of abundant elements. The column densities in these lines are so great that one may sample the outermost parts of the wind. In addition to the resonance lines, the UV region also contains subordinate transitions that arise from levels of low excitation potentials.

In this chapter we will report the results of our IUE observations of six WN + OB systems.

Observations

Table 1 lists the Wolf-Rayet stars selected for this study, along with the available orbital parameters. The systems all contain an early WN component (WN4-6), have short orbital periods, are bright enough for short exposure times, and most are known to undergo periodic profile variations in their optical spectra. Two of the systems, V444 Cyg and HD 211853, are eclipsing binaries, though the

TABLE 1: Observed Systems

	V444 Cyg[a,b,c]	HD 90657[d]	HD 186943[e]	HD 211853[e]	HD 94546[f]	HD 193077[g]
Spectrum	WN5 + O6	WN4 + O4-6	WN4 + O9V	WN6 + O	WN4 + O	WN6 + O + 2
Period (d)	4.2124	8.255	9.5548	6.6884	4.83	2.31
$a \sin i$ ($R_\odot$)	35	50	55	(40)	38	–
i °	78	46-67	70	(70)	–	–
T_0 (-2400000)	41164.332	43915.654	43789.24	43690.32	43140.	–

Notes:

a. Cherepashchuk and Khaliullin (1973).

b. Cherepashchuk (1975).

c. Münch (1950).

d. Niemela and Moffat (1982).

e. Massey (1980).

f. Niemela (1982, private communication).

g. Lamontagne et al. (1982).

11

latter is apparently part of a quadruple system (Massey 1981).
Thus, orbital elements for this system may be uncertain. HD 193077
is a proposed triple system, containing a WN6 + compact object in a
close orbit (P = 2.3 days), both of which are in orbit about an OB
star at a considerable distance (Lamontagne et al. 1982).

The observations were carried out with the IUE at NASA/GSFC with
the Short Wavelength Prime (SWP) camera ($\lambda\lambda$ 1200 - 1900 Å), through
the large aperture and in the low dispersion mode. Exposure times
were chosen so as to optimize the count levels in the continuum and
in the N IV 1718 emission line. Hence, He II 1640 was just satu-
rating on most exposures. Low dispersion images were decided
upon in order to maximize phase coverage of the six systems, reduce
the data reduction complications, obtain good signal to noise
images of the weaker targets, and permit accurate positioning of
the continuum. In addition, lines in WR stars are very broad
($\sim$3000 Km s^{-1}) and are thus ~3 resolution elements wide.

The six targets listed in Table 1 were observed on each of
six observing shifts, and an additional 21 SWP images of V444 Cyg
were drawn from the archives of the National Space Science Data
Center.

Data Reduction

Data reduction was conducted at the Regional Data Analysis Facility (RADF), NASA/GSFC. Standard IUE procedures were employed to obtain absolute fluxes, equivalent widths and wavelength positions. Additional flux and wavelength measurements were made directly from calcomp plots. Recorded exposure times of trailed images were divided by 1.07 to correct for the adjusted trail rate (Panek 1980). No correction for interstellar reddening has been applied.

Since we intend to analyze the variability, it is important to discern fluctuations due to the detection and reduction procedures from the actual spectral variations. In addition, we require an estimate of the uncertainties in the measurements of velocity, flux and equivalent width.

As pointed out by Ayres (1982), a sequence of several images exposed to the same count levels can be used to determine the standard deviation of the individual fluxes about the mean, thus taking automatically into account errors resulting from the original image processing. We will apply this procedure to derive a quantitative estimate of the uncertainties in the measurements, and we will use the eight images of HD 193077 to do so. Given our phase coverage, practically no variability in this source was detected in our low dispersion spectra. Thus, it will serve as a "standard" for comparison with the other more variable sources.
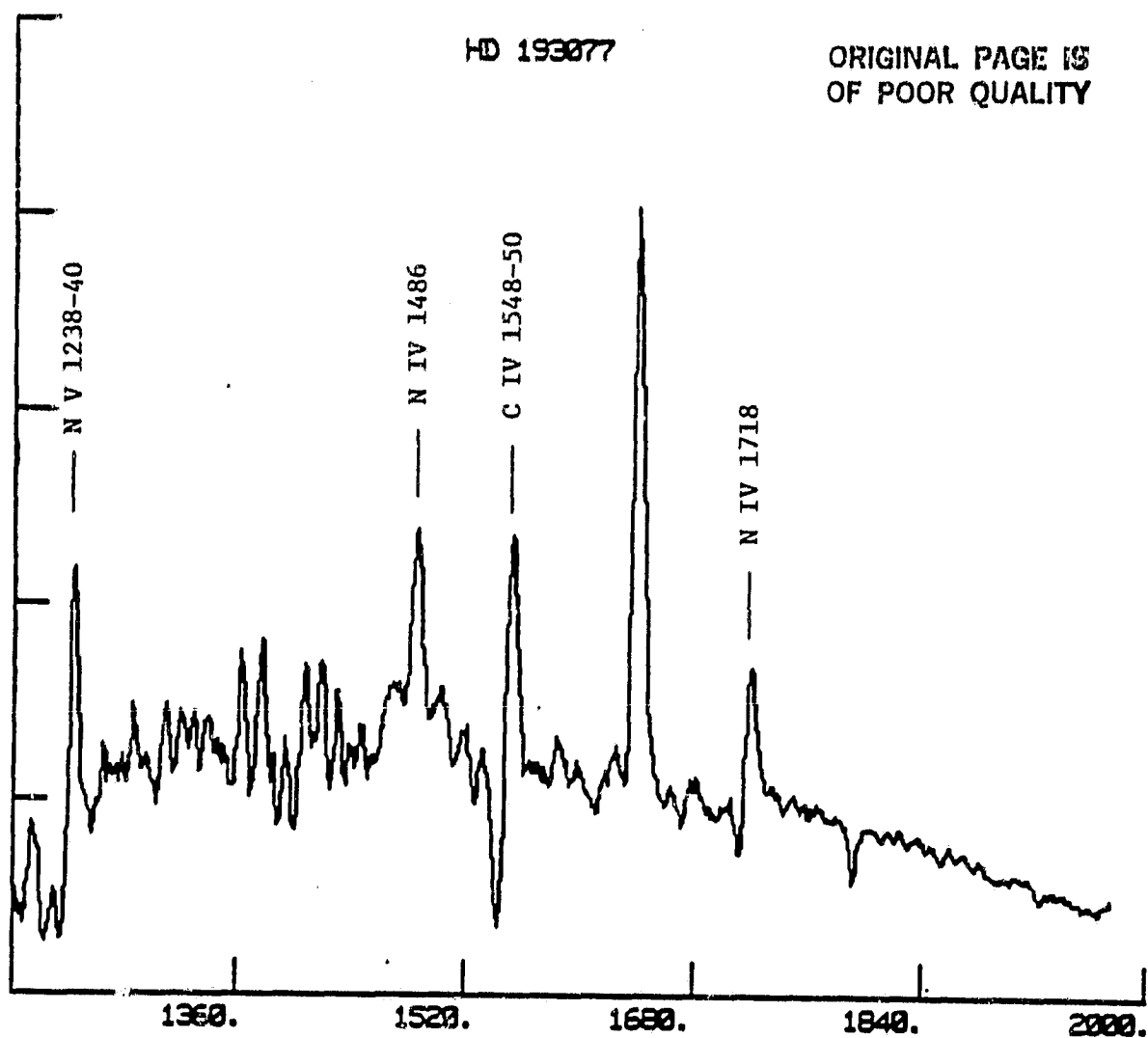
FIGURE 1: IUE spectrum of HD 193077 non-dereddened flux is is given in units of 10^{-11} erg cm^{-2} s^{-1} Å^{-1}, and wavelengths in Angstroms.

In Figure 1 we show the spectrum of HD 193077, obtained
by co-adding the eight images listed in Table 2. The most prominent
emission features are marked. The large concentration of emission
lines is evident in the region $\lambda <$ 1550 Å. Clearly, any analysis
of wind structure requires an unblended line, one which arises in
the WR wind, and sufficiently intense for reliable measurements
to be made. The most promising feature in this respect is the N IV
line at 1718 Å.

In Table 2 we list all the measured quantities for each of the
IUE images, identified by their SWP ("Short Wavelength Prime" camera)
numbers, listed in column 1. SWP numbers smaller than 15500
correspond to images drawn from archives of the National Space
Science Data Center. An asterisk indicates a trailed image. In
column 2 we list the orbital phase computed from the ephemerides
in Table 1. Columns 3 - 5, 8 and 9 contain the positions (in
units of 10^2 km s^{-1}) of the wings and the extrema in flux of the N IV
1718 P Cygni feature, with the following notations: V_1 and V_3
correspond to the blue and red wings, respectively, of the absorption
component: V_5 to the red wing of the emission component; and V_A and
V_E are the minimum in the absorption and the maximum in the emission
respectively. Columns 6 and 10 contain the eye-interpolated mono-
chromatic flux (in units of 10^{-13} erg cm^{-2} s^{-1} Å^{-1}) of the absorption
(F_A) and emission (F_E) extrema, respectively. Columns 7 and 11

TABLE 2: Observed Targets and Measurements

SWP	PHASE	Absorption					Emission				Continuum
		V_1	V_A	V_3	F_A	W_A	V_E	V_5	F_E	W_E	F_{1718}
V444 Cyg											
13832	0.917	-32.	-91.	+1.	8.3	4.8	+9.	30.	21.1	1.9	16.8
14714	0.572	-30.	-23.	-18.	15.0	0.5	-5.	14.	26.6	6.7	16.3
15380	0.852	-23.	-11.	-3.	11.7	1.9	+8	22.	24.7	4.0	17.0
15387	0.992	-22.	-10.	-1.	4.7	4.1	+4.	15.	17.1	2.3	12.2
15388	0.998	-21.	-10.	-1.	4.8	3.9	+5.	20.	17.1	2.8	12.0
15389	0.003	-23.	-12.	-3.	4.5	3.9	+4.	18.	16.9	3.1	11.7
15390	0.008	-20.	-11.	-1.	4.6	4.4	+5.	18.	17.0	2.0	12.2
15391	0.015	-23.	-10.	-1.	5.6	4.2	+7.	20.	18.2	2.2	12.8
15392	0.020	-21.	-10.	0.	4.9	4.2	+7.	18.	17.1	1.8	12.7
15394	0.030	-20.	-10.	-1.	5.7	3.9	+5.	18.	17.5	2.1	12.9
15396	0.051	-17.	-6.	+4.	5.5	4.3	+9.	18.	16.9	0.9	14.5
15397	0.056	-25.	-8.	+2.	5.4	4.1	+9.	16.	17.4	1.2	14.8
15399	0.066	-21.	-7.	+4.	6.5	4.1	+9.	18.	18.1	0.9	15.3
15400	0.071	-39.	-8.	+7.	7.0	6.1	-	-	-	0.0	15.4
15401	0.076	-24.	-6.	+5.	7.2	4.8	+8.	18.	18.4	0.5	16.8
15402	0.081	-19.	-7.	+4.	7.4	3.5	-	-	-	-	15.4

TABLE 2: Observed Targets and Measurements (continued)

SWF	PHASE	Absorption					Emission				Continuum
		V_1	V_A	V_3	F_A	W_A	V_E	V_5	F_E	W_E	F_{1718}
15403	0.085	-24.	-7.	+4.	7.2	4.7	+12	20.	18.8	0.9	16.6
15405	0.098	-25.	-7.	+3.	8.5	4.1	+12.	23.	18.7	1.0	16.4
15406	0.103	-23.	-7.	+5.	7.7	3.9	+11	23.	19.3	2.7	16.5
15407	0.108	-22.	-8.	+2.	7.9	4.1	+10	23.	21.4	2.0	16.6
15408	0.114	-21,	-7.	+4.	8.5	3.9	+11.	22.	20.7	2.0	16.8
15580	0.589	-	-	-11	-	0.	0.	18.	25.0	5.1	15.9
15588	0.835	-24.	-13.	-4.	10.0	2.6	+7.	23.	23.9	2.9	16.5
15602	0.073	-20.	-6.	0.	7.2	3.2	+11.	24.	18.9	1.8	14.9
15615*	0.491	-	-	-10.	-	0.	+5.	24.	19.4	3.9	14.1
15628*	0.736	-31.	-13.	-6.	11.4	2.0	+2.	23.	24.9	4.3	16.3
15644*	0.974	-22.	-11.	-4.	6.3	3.3	+5.	16.	15.8	1.2	12.5
HD 90657											
15576	0.70	-24.	-15.	-6.	6.7	1.4	+2.	18.	11.6	2.8	8.9
11584	0.83	-24.	-13.	-4.	6.3	2.1	+5.	18.	11.9	2.0	9.2
15598	0.95	-40.	-11.	+7.	4.8	4.7	+13.	23.	-	0.6	8.7
15618	0.19	-29.	-9.	0.	6.3	2.7	+9.	30.	14.1	0.6	9.3
15630*	0.31	-20.	-9.	-2.	6.3	1.9	+9.	31.	12.4	4.5	9.6

TABLE 2: Observed Targets and Measurements (continued)

| SWP | PHASE | Absorption | | | | | Emission | | | | Continuum |
		V_1	V_A	V_3	F_A	W_A	V_E	V_S	F_E	W_E	F_{1718}
15646	0.43	-29.	-13.	- 4.	7.8	1.4	+ 7.	24.	12.2	2.9	9.2
HD 186943											
15578	0.11	-23.	-12.	- 5.	5.7	1.8	+ 7.	21.	11.7	4.3	8.3
15585	0.22	-29.	-15.	- 2.	5.8	1.8	+ 7.	31.	13.7	5.8	8.3
15600	0.32	-24.	-15.	- 4.	7.4	0.9	+ 5.	20.	14.0	4.4	8.3
15616	0.52	-	-	-13.	-	-	+ 8.	23.	13.4	5.6	8.3
15627	0.62	-26.	-17.	- 9.	7.3	1.1	0.	18.	13.3	5.5	8.3
15643	0.72	-35.	-2..	-10.	7.0	1.2	+ 2.	23.	13.7	5.1	8.3
HD 211853											
15579	0.38	-20.	- 9.	0.	12.2	1.4	+ 9.	41.	21.2	5.2	15.0
15587	0.53	-18.	- 9.	- 4.	13.9	0.4	+11.	35.	18.9	4.0	14.5
15601	0.68	-26.	-15.	- 2.	14.5	0.8	+ 7.	23.	20.6	3.0	15.6
15617*	0.96	-33.	-11.	+ 5.	9.0	2.9	+20.	45.	16.3	1.6	13.6
15629*	0.11	-26.	- 9.	+ 2.	10.4	2.2	+16.	35.	16.5	2.2	15.2
15645*	0.26	-26.	-11.	- 2.	11.2	2.0	+ 7.	27.	20.4	3.5	15.1

TABLE 2: Observed Targets and Measurements (continued)

SWP	PHASE	Absorption					Emission				Continuum
		V_1	V_A	V_3	F_A	W_A	V_E	V_5	F_E	W_E	F_{1718}
HD 94546											
15577	(0.02)	-	-	-10.	-	0.	+3.	24.	9.0	(7.0)	5.3
15585	(0.23)	-20.	-14.	-8.	4.4	1.1	+2.	21.	8.9	5.9	5.2
15599	(0.43)	-22.	-11.	-4.	4.0	1.4	+7.	34.	7.9	5.6	5.2
15619	(0.85)	-16.	-10.	-5.	4.4	0.7	+6.	23.	9.3	6.5	5.7
15631	(0.06)	-23.	-17.	-9.	5.2	0.4	+4.	19.	9.5	6.2	5.7
15647	(0.27)	-23.	-13.	-6.	4.3	1.4	+4.	17.	9.3	5.6	5.6
HD 193077											
15575*		-21.	-10.	-5.	29.	1.1	+4.	21.	62.6	6.1	39.9
15583		-23.	-10.	-4.	30.	1.2	+4.	22.	64.5	5.2	41.3
15589		-20.	-11.	-4.	27.	1.5	+5.	17.	62.0	6.0	36.7
15597		-18.	-12.	-4.	28.	1.2	+4.	22.	65.0	5.7	37.4
15603		-20.	-10.	-5.	28.	1.3	+6.	21.	63.0	5.4	38.5
15614*		-19.	-11.	-4.	28.	1.5	+4.	21.	66.4	5.5	41.7
15626		-21.	-10.	-3.	32.	1.2	+3	19.	67.5	5.8	38.0
15642*		-22.	-10.	-5.	29.	1.3	+5.	23.	65.4	6.0	42.3

Notes to Table 2

— Asterisk indicates trailed exposure.

— Phases computed from periods and initial epochs in Table 1, the uncertainties in these phases are: 0.002 (V444 Cyg), 0.02 (HD 90657), 0.001 (HD 186943), 0.003 (HD 211853), >0.3 (HD 94546).

— Velocities in units 10^2 km s^{-1}.

— Fluxes in units of 10^{-13} erg cm^{-2} s^{-1} $\overset{\circ}{A}{}^{-1}$.

— Equivalent widths in units of $\overset{\circ}{A}$ngstroms.

— Phases in parentheses have large uncertainties.

contain the corresponding equivalent widths, and finally, column

12 lists the monochromatic flux in the continuum region near the N IV

1718 line, obtained by interpolating the surrounding continuum by

eye.

In the 38 images obtained during our observing run, we, also

measured flux in the continuum region around 1825 $\overset{o}{A}$, which is

relatively free of lines. The averages $\pm$ standard deviations for this

quantity (F_{1825}), V_A, V_E, F_A, F_E, W_A, and W_E are listed in Table 3.

The "%" sign indicates percent variations; i.e., (s.d.)/mean.

According to the results in Table 3, we can state that, with respect

to HD 193077, there is significant line flux and equivalent

width variability in V444 Cyg, HD 90657, HD 211853, and moderate

variability in HD 186943 and HD 94546. On the other hand, little or

no continuum variability is detected. It is interesting to note

the large difference between the velocity standard deviations in

HD 193077 and those of the reset of the sources. Specifically

we find the standard deviation of relative measurements to be

~90 km s^{-1} from the HD 193077 values. This illustrates the remarkable

stability of the IUE wavelength calibration procedures, and quantifies

the uncertainty in establishing the position of extrema in the P

Cygni profiles. Thus, although velocity measurements are limited

in general by the ~6 $\overset{o}{A}$ resolution of the low dispersion spectra,

position of extrema (i.e., line centers) can be determined with much

)

TABLE 3: Averages and Standard Deviations

TARGET	$\langle V_A \rangle$	$\langle V_E \rangle$	$\langle F_A \rangle$	%	$\langle P_E \rangle$	%	$\langle F_{1025} \rangle$	%	$\langle W_A \rangle$	%	$\langle W_E \rangle$	%
V444 Cyg[a]	−11±3	+ 5±4	10 ±3	30	21 ±4	18	11.9±1.1	8	1.8±1.5	80	3.2±1.5	50
HD 90657	−11±2	+ 7±4	6 ±1	17	12 ±1.3	11	7.4±0.1	1	2.4±1.2	50	2.7±1.2	50
HD 11146	−13±3	+ 4±2	4.5±0.4	10	9 ±0.8	6	4.4±0.1	3	0.8±0.6	80	6.1±0.6	10
HD 186943	−16±3	+ 4±3	6.8±0.8	12	13.3 ±0.8	6	7.3±0.1	2	1.1±0.8	70	5.1±0.4	10
HD 211853	−11±2	+12±5	11 ±3	27	19 ±2	11	12.5±0.6	5	1.6±0.9	58	3.2±1.3	40
HD 193077	−11±0.7	4±0.3	28 ±1	4	64 ±2	3	31.2±0.3	1	1.3±0.1	10	5.7±0.3	5

Notes:

a. Data only for the 6 SWP images obtained in our observing run.

higher precision. Furthermore, the stability of the wavelength calibration permits relative flux measurements at a given wavelength to be obtained with considerable reliability. We emphasize that our present analysis will require only relative flux and wavelength measurements. The velocity standard deviations in all the other sources are ~200 - 300 km s^{-1}, comparable with typical orbital velocities reported for WR stars.

Ultraviolet Variations

Figures 2 (a) - (e) illustrate the UV spectra at individual orbital phases of the five variable sources. The variations can be summarized as follows:

a) The P Cygni structure of N IV 1718 Å undergoes a transition from a strong emission accompanied by a weak or absent absorption component when the WR is in front of the O-star ($\phi \sim 0$) to weak or absent emission with a shortward-shifted, very intense absorption component at the opposite phase.

b) He II 1640 develops a shortward-shifted absorption component at $\phi \sim 0$, but no absorption is apparent at other phases.

c) The apparent continuum region shortward of ~1500 Å is significantly depressed at $\phi \sim 0$. In the more extreme
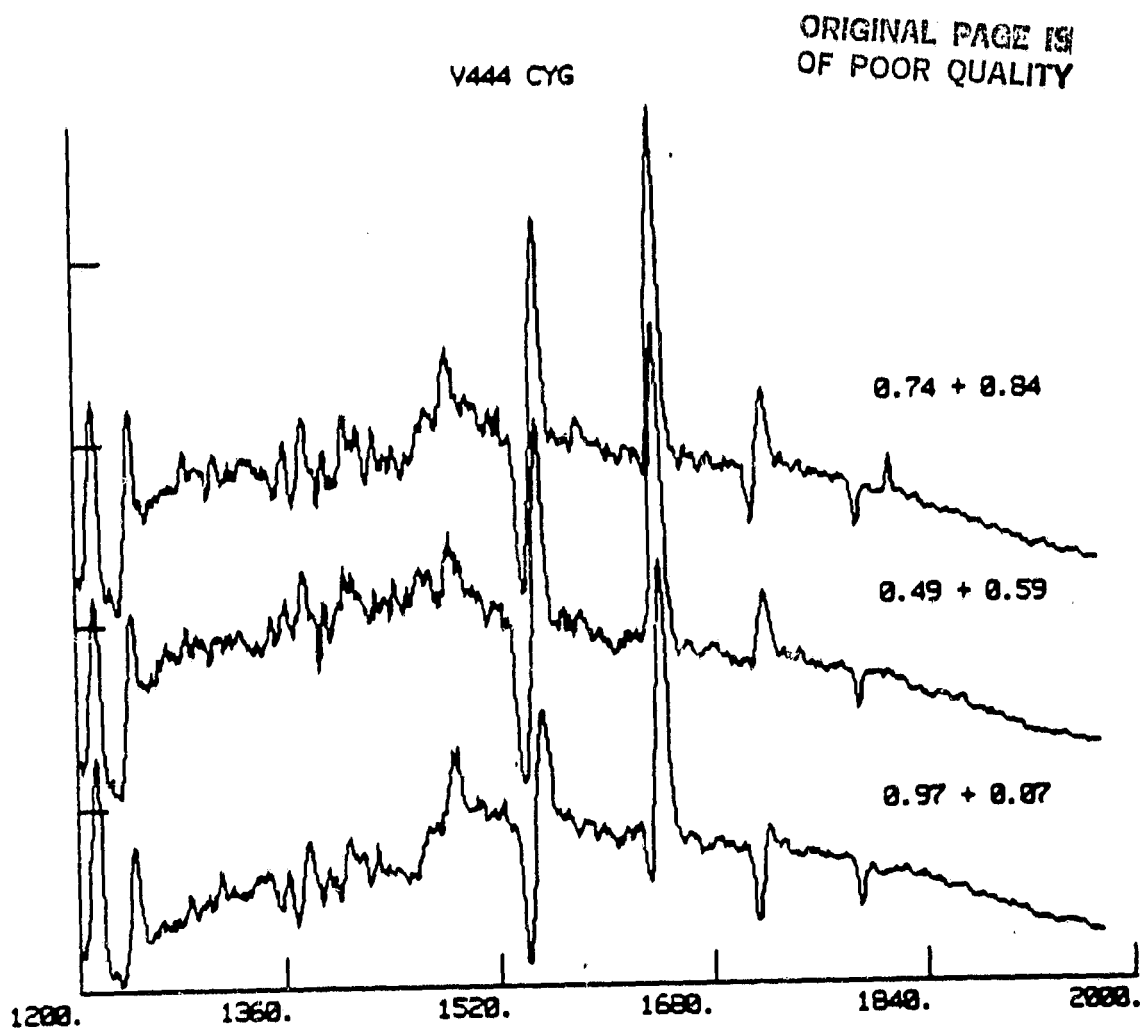
FIGURE 2(a): IUE spectra of V444 Cyg. Spectra at similar orbital phases have been co-added, and are identified by these phases.
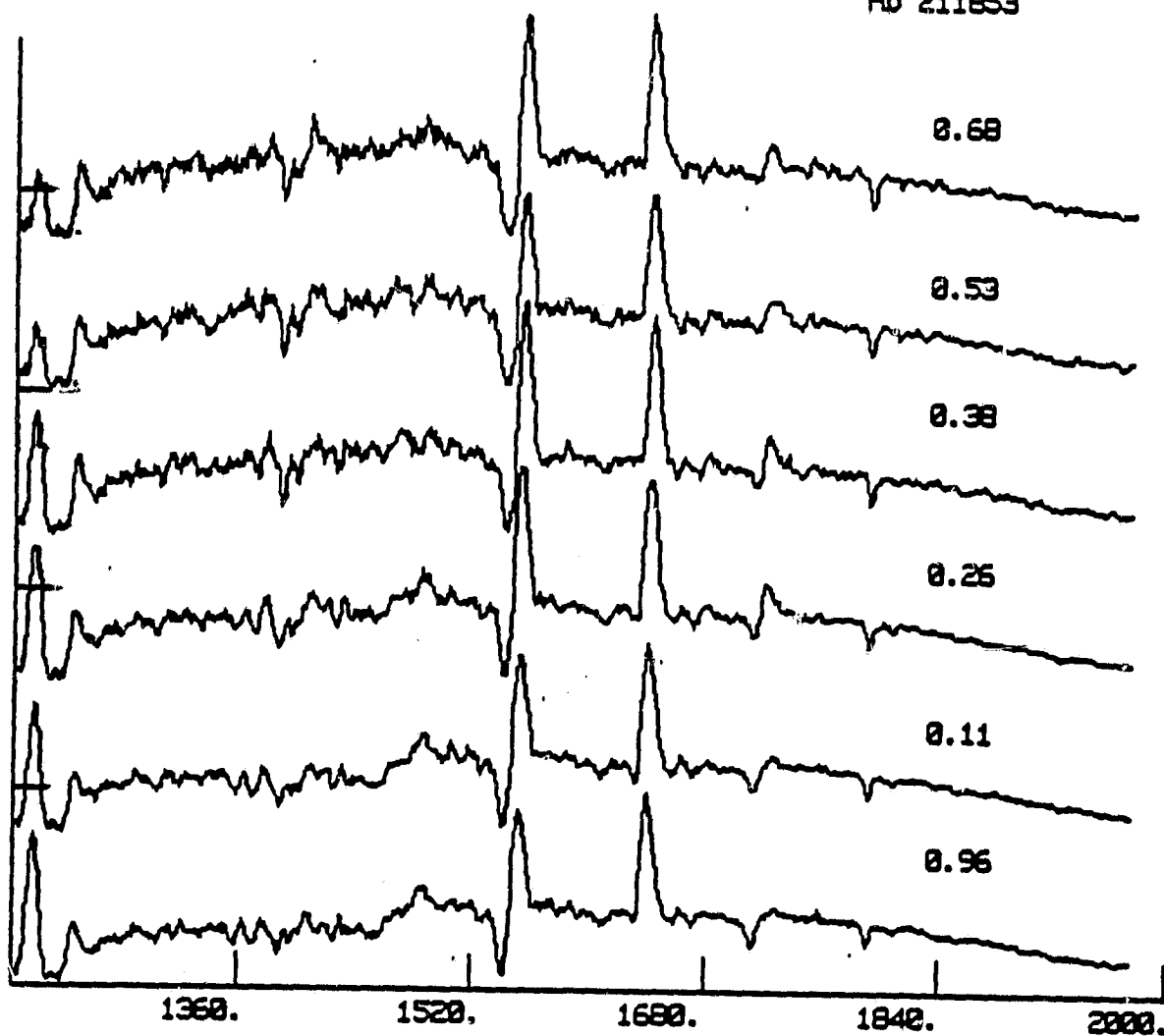
FIGURE 2(b):   Individual IUE spectra of HD 186943 identified by orbital
phase.
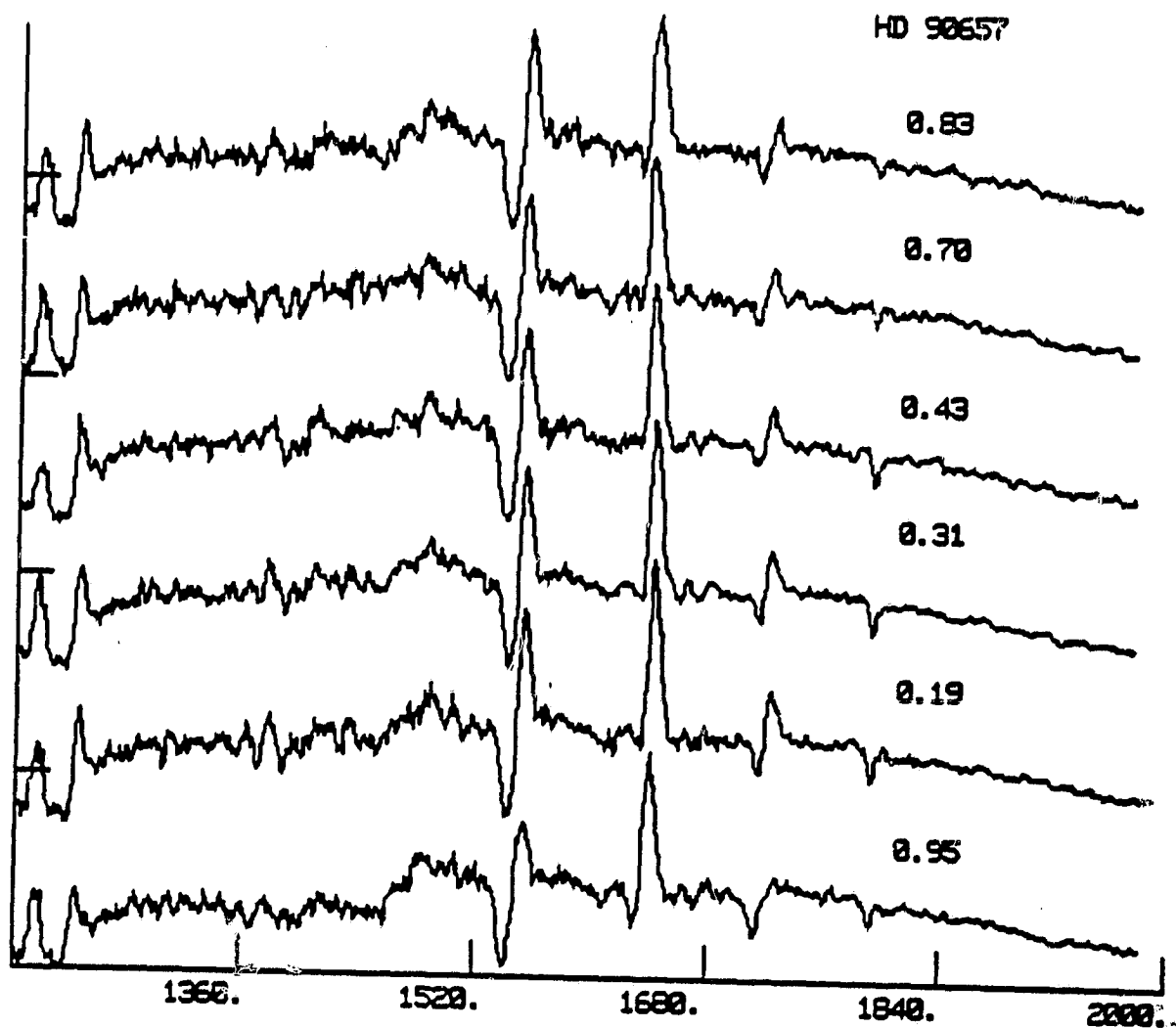
FIGURE 2(c): Individual IUE spectra of HD 90657 identified by orbital
phase.
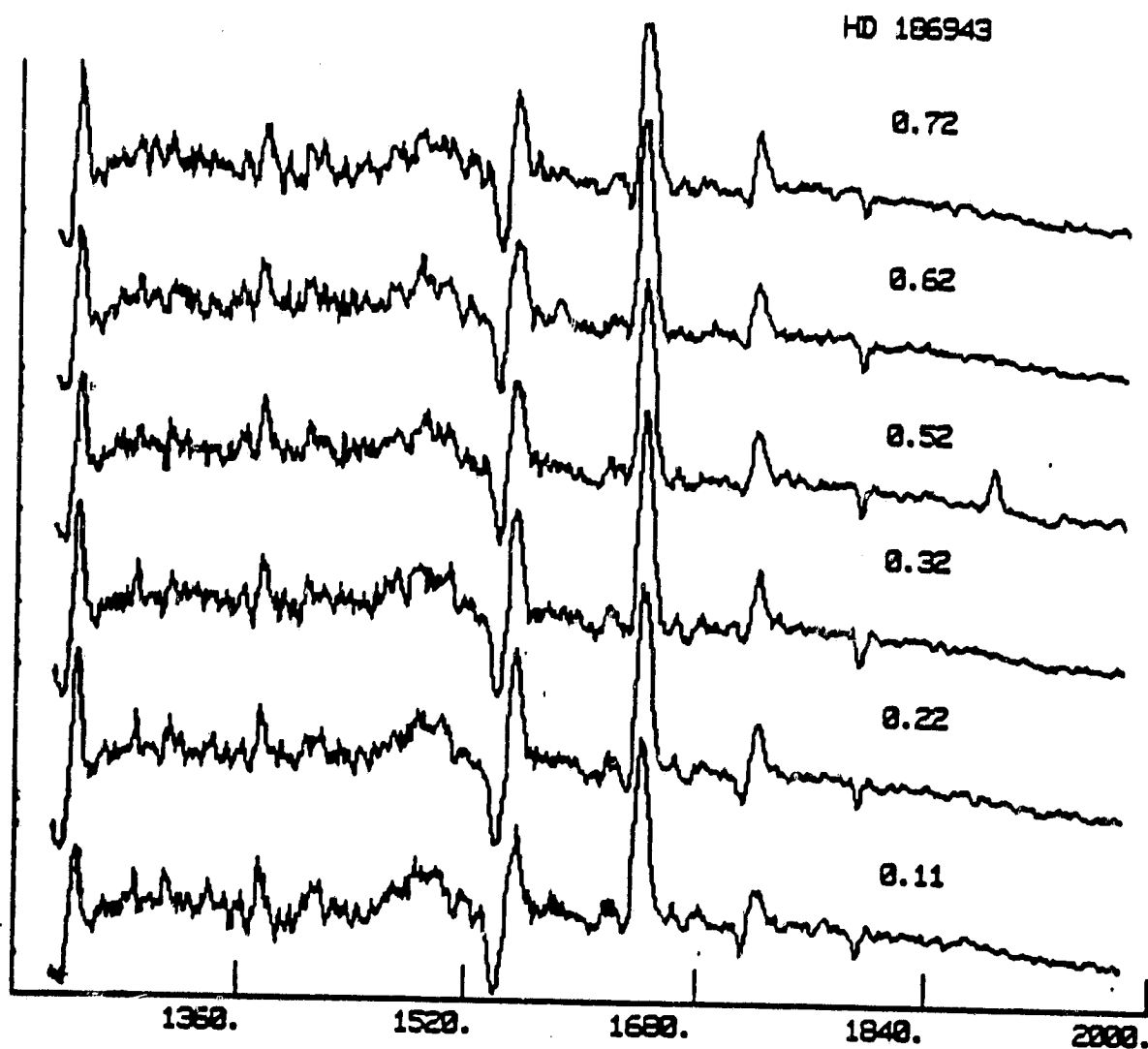
FIGURE 2(d):   Individual IUE spectra of HD 211853 identified by orbital
phase.
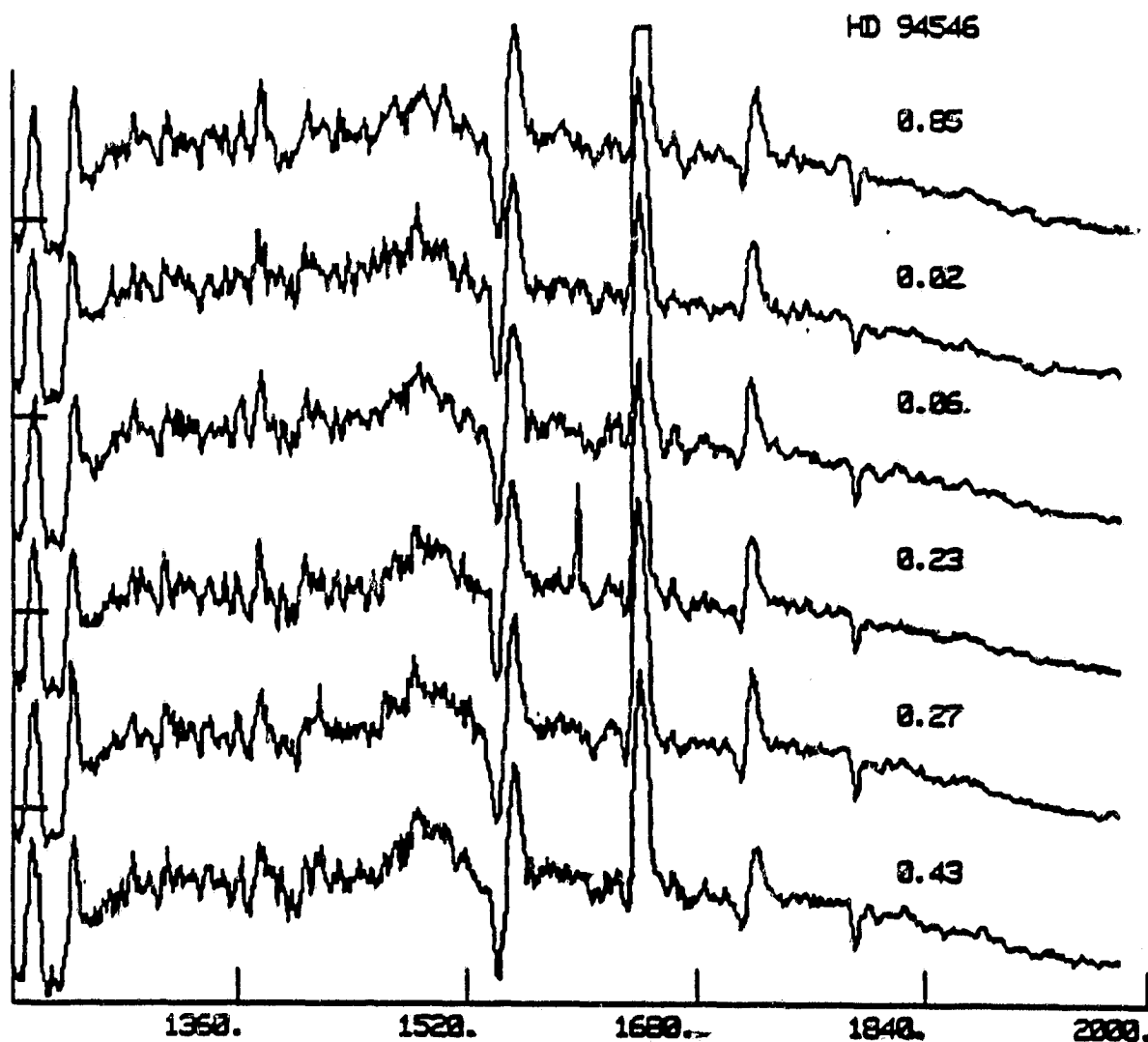
FIGURE 2(e):   Individual IUE spectra of HD 94546 identified by orbital
phases computed with data in Table 1.   By analogy with
the previous systems, we have placed the spectrum with
strongest absorption (labeled with phase 0.43) on the
bottom

cases this constitutes a variation of 45% in flux

level, while no variations greater than 8% occur in

the 1825 continuum region in the same images.

d) The emission component of C IV 1550 shows a decrease in

intensity at $\phi \sim 0$, but at the same time the absorption

component is narrower instead of broader and deeper, as

occurs with the N IV 1718 line.

As already mentioned, the strongest variations are seen to

occur in V444 Cyg, HD 90657 and HD 211853, though a more complete

phase coverage of the other two sources may disclose similar degrees

of variability. There is no evidence for continuum eclipses in any

of the sources except V444 Cyg, where the additional images obtained

at $\phi = 0$ display variations consistent with the 30% eclipses observed

in the optical region ($\lambda\lambda$ 4200 - 7500 $\overset{o}{A}$; Cherepashchuk and Khaliullin

1973). The continuum eclipses are significant at $\phi = 0.0 \pm 0.03$.

Thus, the variations at emission line frequencies occur over a wider

phase interval than the continuum eclipses, as would be expected from

selective atmospheric eclipses.

Interpretation

Basically, we can describe the observed UV variations as

the presence of strong absorptions at $\phi \sim 0$ and their decrease

or disappearance at the opposite phase. This is exactly the same

behavior that has ben reported for the optical region in a few
WR binaries (c. f. Münch 1950; Cowley et al. 1971), and we will
establish a suitable explanation for these variations in terms
of selective atmospheric eclipses.

According to this interpretation, as the O-star passes
behind some portion of the WR wind, its continuum radiation is
absorbed by ions in the wind. The absorption occurs at frequencies
corresponding to atomic transitions with favorable transition
probabilities whose lower levels are adequately populated.
In this respect, these frequencies are selected for absorption, while
others are not affected. However, because of the large expansion
velocities in the winds, a relatively wide range of frequencies will
be affected, as we will explain below.

For a given transition, each frequency that we observe in an
emission line is emitted by material located on a constant velocity
surface, which will have a large geometrical extension (see e. g.
Mihalas, 1978, Ch. 14). However, the absorption of the O-star's
continuum can only arise in a narrow cross-section of the constant
velocity surfaces, which lies along the line-of-sight between the
observer and the O-star.

Figure 3 illustrates the geometrical setting of this
discussion. The wind expands spherically about the WR core, which
is at the center of the (p,z) - coordinate axes system. The degree
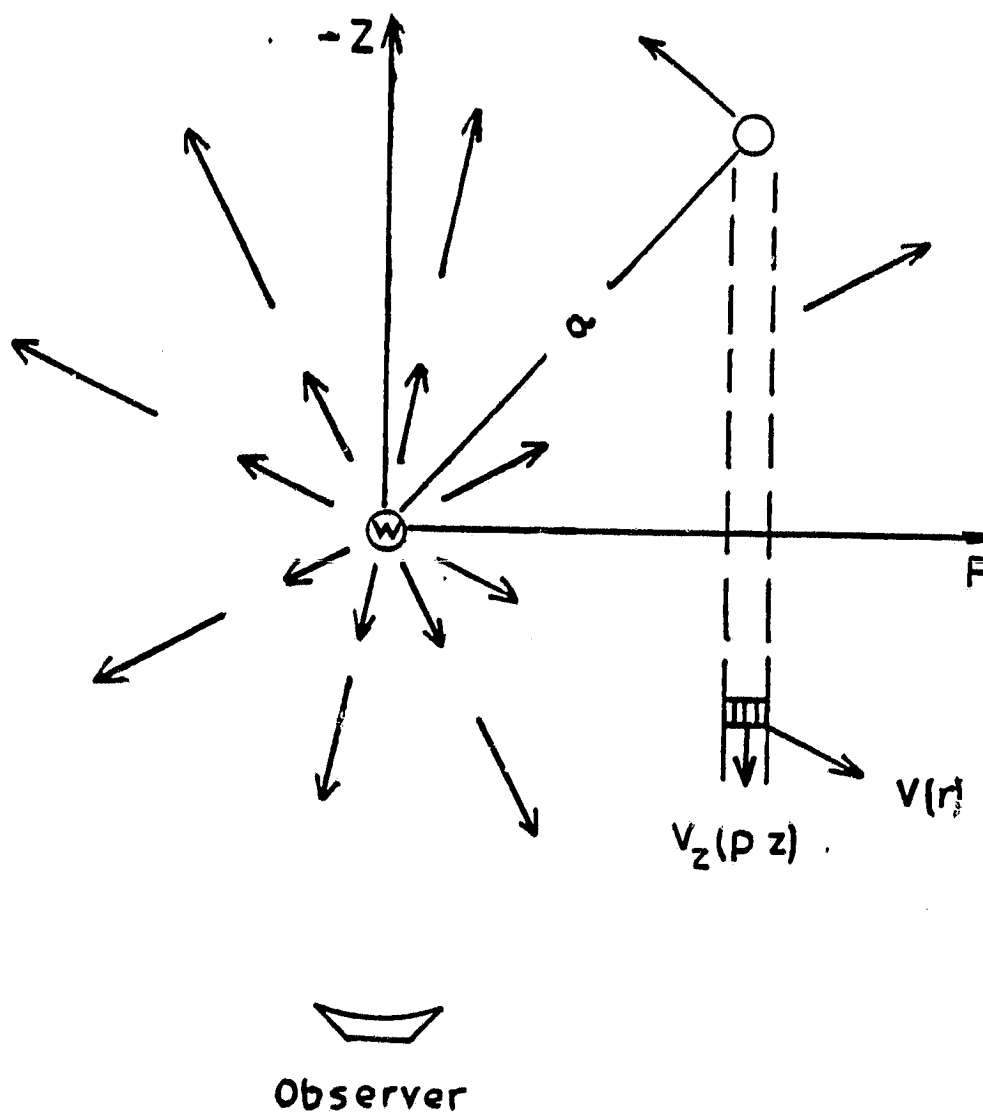
FIGURE 3: Simplified interpretation of the geometric setting giving rise to the phase dependent variations.

to which the absorption occurs at each frequency depends upon the optical depth along the line-of-sight to the O-star at that frequency, and this depends entirely upon the opacity of the material, $\chi(r)$, and the velocity gradient in the wind. That is,

$$\tau = \frac{\chi(r)}{\frac{dVz}{dz}} = \frac{\chi(r)}{\mu^2 \left(\frac{dV(r)}{dr} \right) + \frac{V}{r}} \qquad \ldots\ldots 1$$

where $V_z = V(r)\,(z/r)$, $\mu = z/r$, and $r = (p^2 + z^2)^{\frac{1}{2}}$. The opacity contains known atomic constants and the level populations:

$$\chi(p) = \frac{\pi e^2}{mc} \; (gf\lambda) \left[\frac{N_1}{g_1} - \frac{N_u}{g_u} \right] \frac{1}{v_{th}} \qquad \ldots\ldots 2$$

where N_1, N_u are the poulations of the lower and upper levels of the transition, respectively. The relevant velocity gradient in equation 1 is the change in the z-component of the expansion velocity in the z direction (i.e., along the line of sight).

Consider an orbital phase such as that illustrated in Figure 3. If we assume that the emitting material extends out to a distance $z = Z_{max}$, all the material along the p=P = constant ray, from $z = 0$ to $z = +Z_{max}$, will absorb radiation from the O-star at wavelengths ranging from λ_0 to $\lambda_0 (1 - \frac{1}{c} V_z(P, Z_{max}))$. Hence, λ_0 is the wavelength of the transition in question in the rest frame of the WR star. Therefore, this will generate a shortward-

shifted absorption. However, the material having a z-component velocity toward the O-star (i.e., $V_z(-z)$) can also absorb, and will do so at wavelength longward of λ_0. The maximum "redshifted" absorption will have a wavelength $\lambda_0(1 - \frac{1}{c} V_z(P, -Zu))$ where $-Zu$ corresponds to the closest point to the O-star at which the WR wind structure is unmodified by the companion's presence.

As the orbital phase varies, the impact parameter P does too, which leads to a varying range in V_z values. Thus, as one proceeds from orbital phase 0.75 to 0.0, wind material with a growing range of V_z values occults the O-star, and thus a progressively broader absorption is predicted.

We must note that because we are dealing with ionic transitions, the opacity does not depend solely on the overall density distribution in the wind but also on the excitation conditions. Even if the density and temperature distributions decrease monotonically with distance, the population at the lower level of the transition (which gives rise to the absorption) may not. Hence, the opacity for the given line may have a maximum at a certain distance from the stellar core, and this distance may vary for different transitions, depending on the excitation potentials. In Chapter III we will derive a non-monotonic optical depth distribution.

Alternatives to the selective atmospheric eclipses interpretation have been proposed, and rely on the presence of streams of

material or on a "heating" effect in the WR hemisphere facing the
O-star. In the first scenario, gas streams flowing through the
Lagrangian points of the gravitational equipotentials of the system
(Sahade 1958; Kuhi 1968) produce enhanced absorption at the
appropriate orbital phases. However, WR + OB binary systems do not
comform to a simple Roche Lobe. overflow geometry. First of all,
the large wind velocities prevent the equipotential surfaces from
having a significant effect on the mass outflow (Castor 1970b).
Secondly, we now know that all OB stars have considerable mass out-
flows of their own, leading to a wind-wind collision in the region
between the WR and OB members of binary systems. The energy re-
leased in this collision (Prilutskii and Usov 1976; Cooke et al.
1978) renders any interpretation in terms of "cool" streams of
gas extremely unlikely. The second interpretation is somewhat
related to the possible wind-wind collision. Many of the variations
observed in WR binaries have led the observers to infer the presence
of "hot" material located between the two members of the binary
system (Kuhi 1968; Khaliullin and Cherepashchuk 1975). We will show
that there is indeed evidence for a wind-wind collision in our
observations, but that the effects of this interaction are secondary
to those of the atmospheric eclipses.

Figures 4(a) and 4(b) show the phase dependence of the
emission and absorption equivalent widths, respectively. V444 Cyg,

FIGURE 4: Equivalent widths of the (a) emission and (b) absorption
           components of N wV 1718 as a function of orbital phase.
           In (c) we plot the ratio of absorption to emission equiva-
           lent width as a function of phase, for comparison with
           this ratio in HD 193077, represented by the filled-in
           square. Other symbols correspond to close WN + OB systems
           and represent: . V444 Cyg, o HD 211853, x HD 90657 and
           + HD 186943.
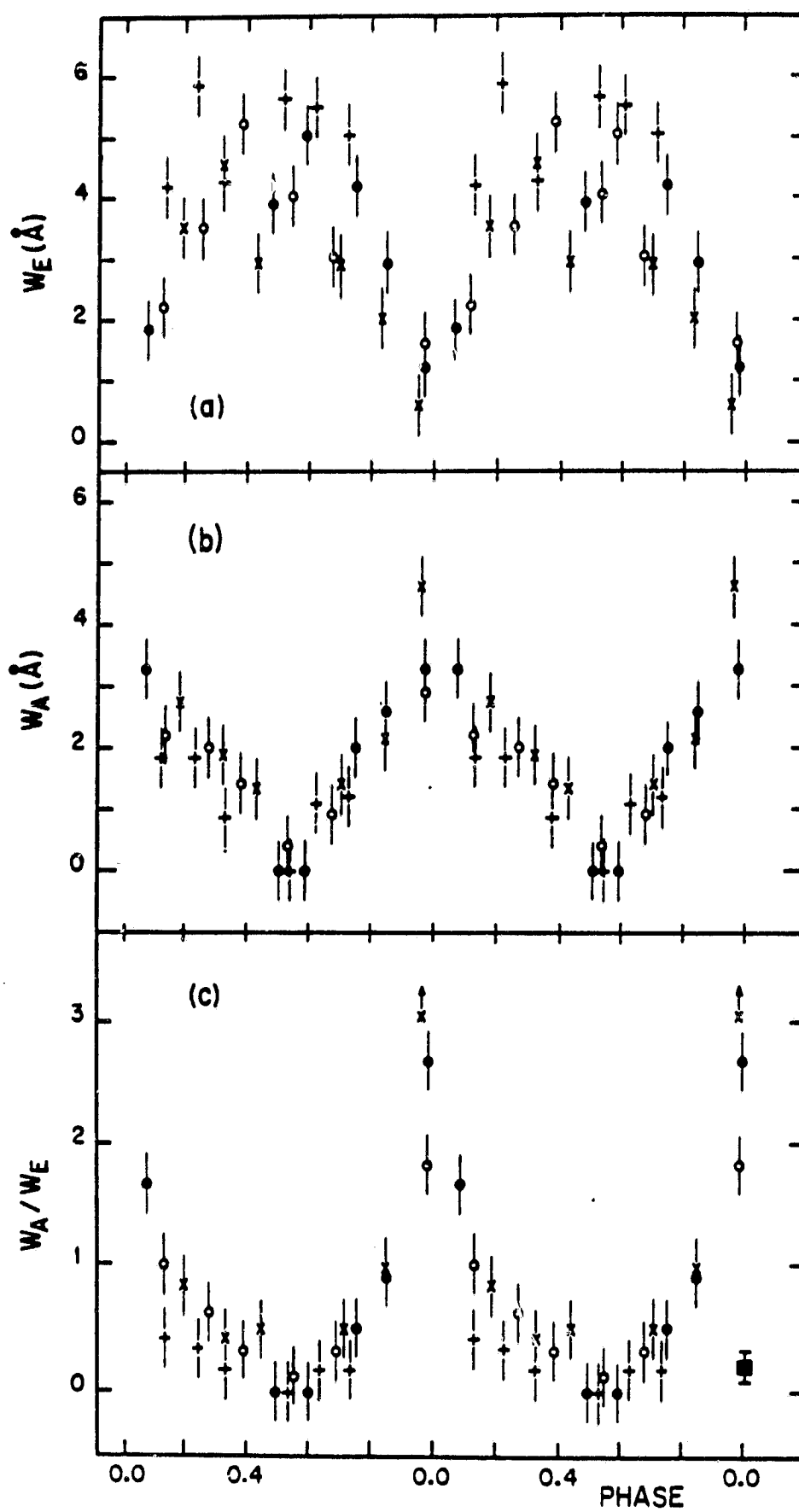
HD 90657, HD 211853 and HD 186943 are repesented on the same scale, with different symbols. The similarity in the W_A amplitude is striking, and apparently reflects the similarity of the WN winds in these cases. The gradual decrease in W_A as the O-star come out from behind the WR wind, accompanied by a gradual increase in emission indicates that the variations observed in the emission component are directly related to those in the absorption component.

The ratio W_A/ W_E as a function of orbital phase is shown in Figure 4(c). The filled-in square represents the value of this ratio derived from the HD 193077 spectrum. Since perturbations due to a close OB companion are minimal in this source, its W_A/W_E value is closest to that expected from an unperturbed WR P Cygni feature, and can be used for comparison with the other sources. Thus, we may conclude that in the four variable sources, the N IV 1718 line is altered by enhanced absorption during orbital phases $0.8 < \phi < 1.2$, and perhaps reduced absorption at the opposite phases (i.e., $\phi \sim 0.5$). The ratios are equal to the HD 193077 value at elongations, which tells us that radiative interaction effects at these phases are negligible.

The variations resulting from selective atmospheric eclipses can be modeled using the computer code described in the Appendix, and compared with the observational data. In Figure 5 we have constructed an $\epsilon - \alpha$ plot for the N IV 1718 line using the data

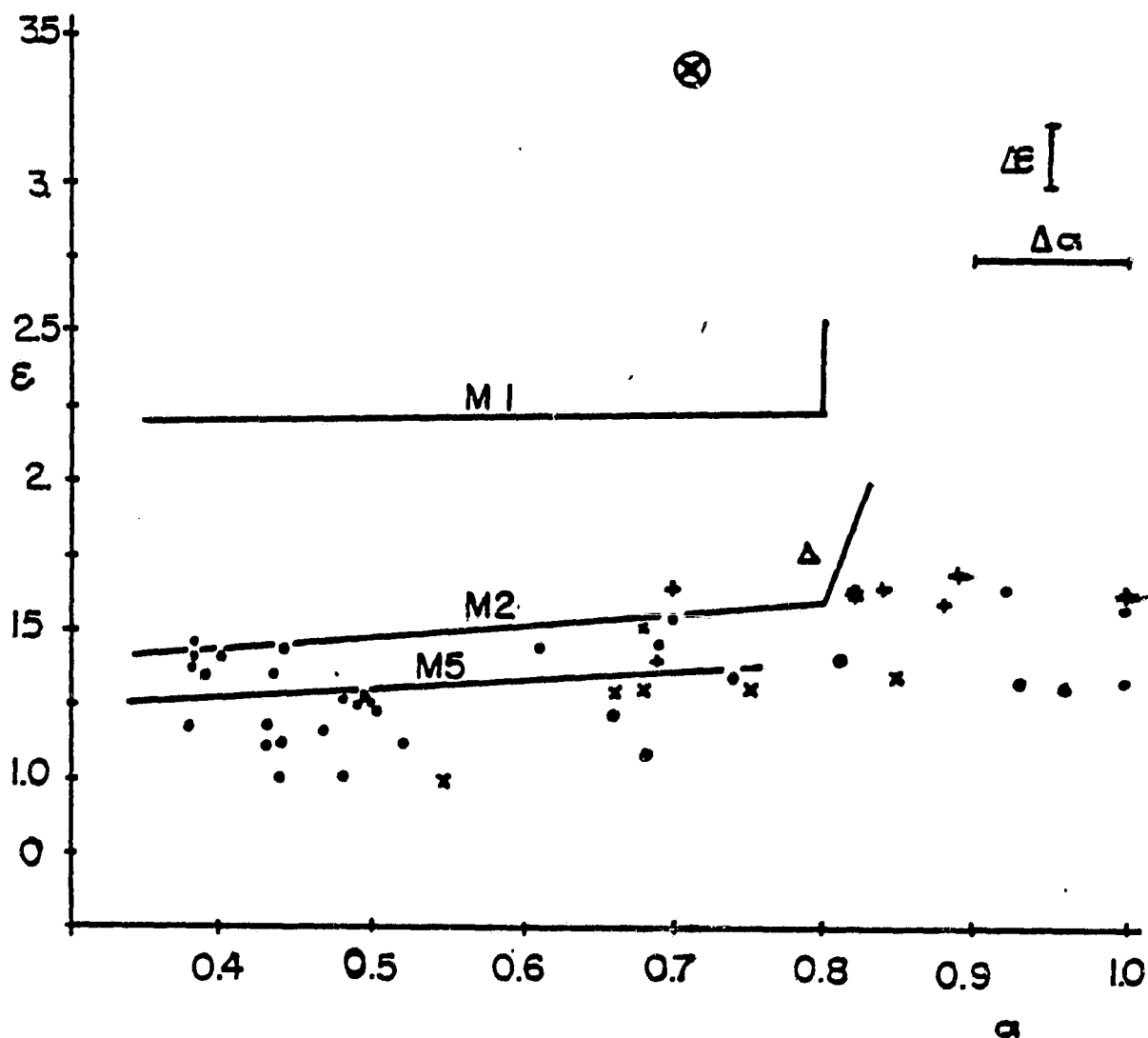FIGURE 5: Comparison of model derived and observed (α,ε) values.
Curves marked M1, M2 and M5 correspond to models with $L_w \div L_o$
intensity ratios of 1:1, 1:2, and 1:5, respectively.
Different symbols represent the different WN targets:
. V444 Cyg, o HD 211853, x HD 90657, + HD 186943, * HD 94546,
Δ HD 193077 and X HD 50896. Δε and Δα are the propagated
uncertainties in the ε and α measurements, respectively.

in Table 2. As in the Appendix, $\varepsilon = F_E/F_C$, and $\alpha = F_A/F_C$, where F_C is the measured continuum level in the region of the emission line. Different symbols represent the different sources. For a given WN + OB binary system, there is a large spread in α values, which results from the phase-dependent variations of the absorption component. Thus, at $\phi \sim 0$, $\alpha = 0.4 - 0.5$, increasing to $\alpha = 0.7 - 0.8$ at elongations and approaching unity (i.e., $F_C \approx F_A$) at $\phi \sim 0.5 - 0.6$. The encircled "X" symbol on this plot represents HD 50896 (SWP 13844 + SWP 14136), whose value differs considerably from those of the other systems (including HD 193077). HD 50896 is a system containing a WN5 Wolf-Rayet and a degenerate companion thought to be a neutron star (Firmani et al. 1980). In this case, the continuum level can be regarded as arising in the WN5 component of the system. In addition, the N IV 1718 line does not undergo variations like those we have described for the WN + OB systems (Rumpl, private communation).

We have used the (α, ε) position of HD 50896 to determine the value of opacity at the surface of the core (CO) and the relative intenstiy of the continuum with respect to the emission line (PRIM) according to the procedure outlined in the Appendix. The computer code was run with these quantities, the additional parameters as listed in the Appendix (i.e., constant velocity law, etc.) and WN : OB intensity ratios of 1:1, 1:2, and 1:5.

The curves in Figure 5 corresponds to the resulting model values of (α,ε) pairs for orbital phases ranging from just past elongation ($\phi = 0.75$) to just before geometrical eclipse of the O-star by the WR ($\phi = 0.0$), and are labelled according to the relative intensity of the O-star. Near elongations, $\alpha \sim 0.7 - 0.8$, while near $\phi = 0$, $\alpha = 0.4$, in very good agreement with the data. The dependence of ε on the relative intensity of the O-star is evident, and the best agreement with the data is achieved with the M5 model. This corresponds to a 1:5 intensity ratio, as expected from optical eclipse observations of V444 Cyg (Kuhi 1968). However, model ε values become rather insensitive to relative values of WN : OB greater than 1:5, and thus we can only set a lower limit to the intensity ratio.

In conclusion, we show that by a) adopting wind parameters from HD 50896, b) including a luminous companion, and c) assuming selective atmospheric eclipses of the companion by the WN wind we can reproduce observed (α,ε) values for orbital phases $0.8 < \phi < 1.2$. We are unable to generate the values of α observed at phases $\phi \sim 0.5$, when our model does not take into account any "heating" effects or the finite diameters of the two opaque, continuum-emitting cores. In addition, we have assumed that the spectral classification represents actual physical conditions in the winds, and that therefore we can apply informaion derived from one system (i.e., HD 50896) to other, slightly different systems.

In summary, we have presented results of empirical and semi-empirical tests, both leading to the conclusion that selective atmospheric eclipses provide a satisfactory explanation for the dominant phase dependent spectral variations observed in WR + OB binaries. We will now consider some of the second order effects of this interpretation, and in the next chapter obtain an optical depth distribution for the winds of our sample of WN stars.

Wind - Wind Collisions

In Figure 6(a) and 6(b) we have plotted the ratios of the images corresponding to "WR in front" divided by "O-star infront" for the five variable systems. Where possible, spectra corresponding to similar phases have been co-added to increase the signal-to-noise factor. For HD 94546 it has been necessary to construct the ratio with the spectrum corresponding to $\phi \sim 0.5$ in the numerator; i.e., inverted with respect to the other cases . We note, however, that an error of 0.006 day in the orbital period, which is consistent with uncertainties in the period determination, could generate a phase shift of 0.5 when extrapolating zero phase from the initial epoch listed in Table 1 to the observations reported here.

The changes in the spectra between phases near 0.0 and 0.5 are evident in Figure 6. For example, the enhanced absorptions at $\phi \sim 0$ show up here as depressions with respect to the level of
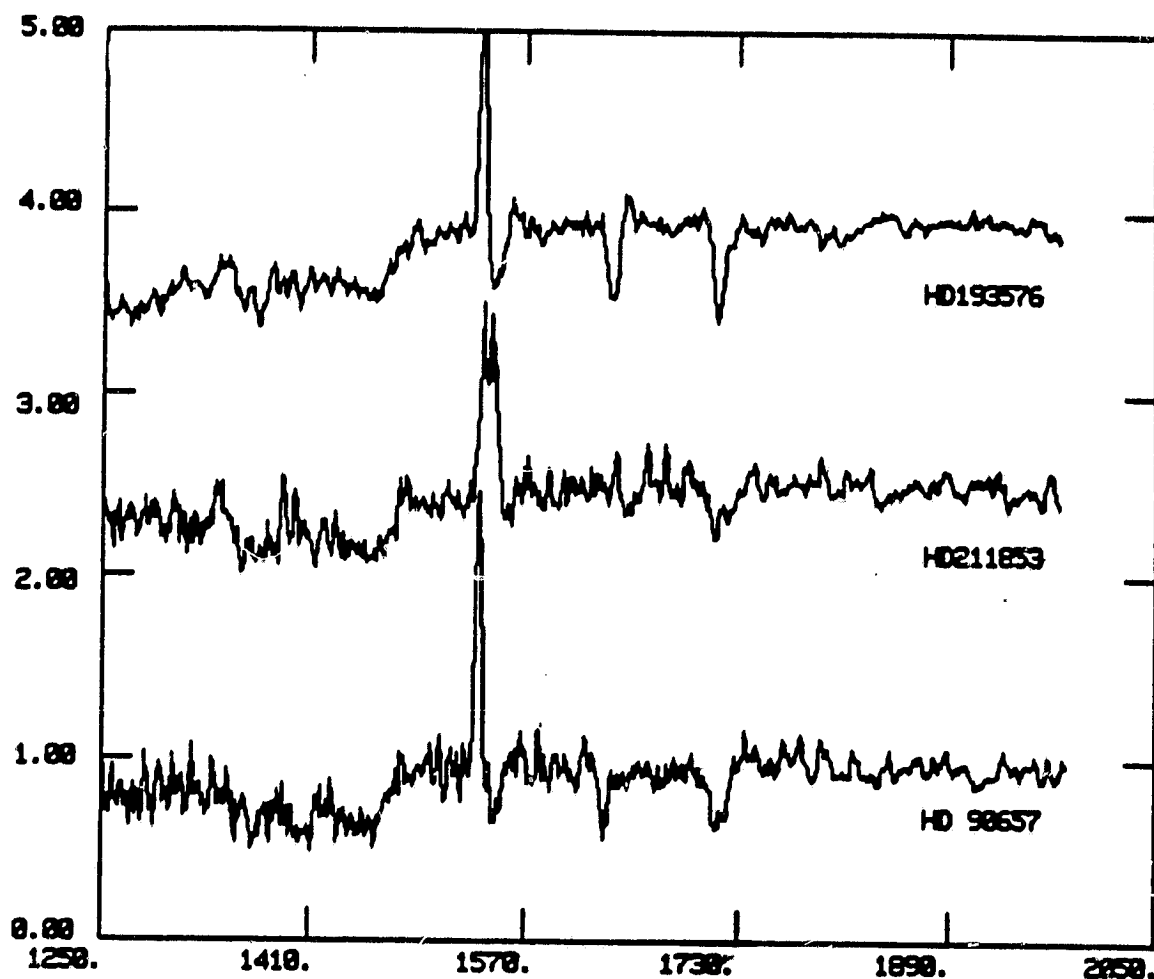
FIGURE 6(a): Ratios of images corresponding to "WR in front" divided by "O-star in front". The images used in each case are: (SWP 15602 + SWP 15644)/(SWP 15580 + SWP 15615) for V444 Cyg, (SWP 15617)/(SWP 15629) for HD 211853, (SWP 15598)/ (SWP 15646) for HD 90657. Ratios are displaced vertically with respect to each other by 1.5 units.
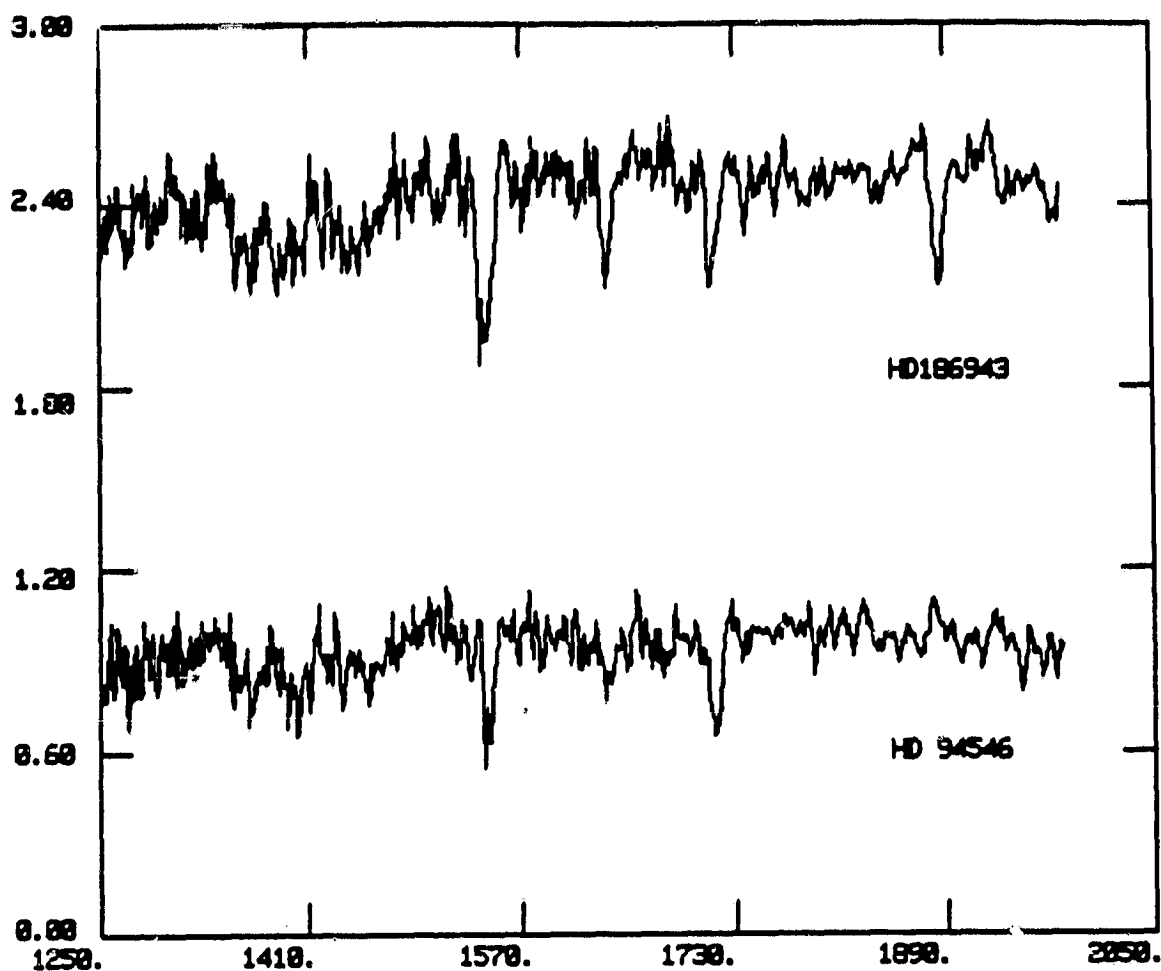
FIGURE 6(b):   Ratios of images as in Figure 6(a), corresponding to:
(SWP 15578)/(SWP 15616) for HD 186943, and (SWP 15599)/
(SWP 15631 + SWP 15577) for HD 94546.

unity. That is, if there were no variations, the ratios would be equal to unity at all wavelengths. Particularly striking is the spike at ~1540 Å in Figure 6(a), which results from the narrower C IV 1550 absorption component at $\phi \sim 0$, as compared to $\phi \sim 0.5$. Since this line corresponds to a resonance transition, it can produce absorption even at extremely low densities (c. f. interstellar medium), and thus, a strong contribution from the O-star's wind to the overall profile is expected. The fact that the absorption is broader when the O-star is in front of the WR implies that the O-star's contribution occurs at higher expansion velocities than the contribution arising in the WR wind. This means that the O-star companions in the systems of Figure 6(a) have C IV out to higher wind velocities than do the WR's. Published results for terminal velocities in O-stars (Garmany et al. 1981) and in WR's (Barlow et al. 1981) suggest that the early O-stars do indeed have higher terminal velocities. Though adequate phase coverage is lacking, it may be significant that the spike is absent in the HD 186943 ratio, since this system contains the latest O-type companion of our sample.

Strong wind-wind interaction effects are suggested by the curious behavior of the shortwardmost edge of C IV 1550. That is, the fact that the high-velocity portion of the absorption is present primarily when the O-star is in front of the WR, and

diminishes when it is in back implies that the O-star's wind structure is disturbed. In the case of a wind-wind collision, the interaction would affect primarily the outermost portions of the O-star's wind, which is where maximum expansion velocities have already been reached. Because the outflow from the WR is more massive than that of the O-star, the former is expected to dominate, and one can envision the O-star's wind being stopped, and the ionization structure of its outer portions altered by the collision. Thus, the spikes in Figure 6(a) provide observational evidence for wind-wind collisions in WR + OB binaries.

Figures 2(a), (b), and perhaps (c) suggest that the alteration of the O-star's wind may not be limited to the hemisphere facing the WR star. In these figures, the C IV 1550 absorption appears to be narrower close to elongation, as well as at $\phi \sim 0$, though this may be a result of the relative orbital motions.

Evidence from X-ray observations for the existence of wind-wind collision regions in WR binaries may exist (Sanders, Cassinelli and van der Hucht, 1982) since the X-ray spectral distribution of one source (γ Vel) is harder ($T \sim 10^7$ K) compared to other WR sources. The latter's spectral distribution appears to be consistent with the X-rays being generated by small shocks within the stellar wind (Lucy and White 1982).

Possible Fe V and Fe VI Contributions

With the exception of V444 Cyg at orbital phases $\phi = 0.00$ $\pm$ 0.03, no appreciable changes in the continua at $\lambda > 1550$ Å occur in our SWP images nor in LWR (Long Wavelength Redundant, $\lambda\lambda$ 1900 - 3300 Å) spectra of HD 211853 and HD 18943 (Hutchings and Massey 1983). However, changes shortward of 1500 Å are significant, especially in systems of Figure 6(a). These changes are approximately of the same magnitude as those in N IV 1718, and have the same phase dependence. Thus, it is very probable that they result from line variablity. That is, closely spaced, numerous lines all behaving in the same manner would, given their Doppler broadening, produce the observed effects. In fact, there is a large concentration of lines at $\lambda < 1550$ Å, most of them due to transitions of Fe V and Fe VI ions, as a search through published line lists (Reader et al. 1980; Ekberg 1975a, 1975b; Ekberg and Edlen 1978) can easily show. Specifically, Fe V has 236 lines within the wavelength interval $\lambda\lambda$ 1300 - 1500 Å, but only 78 weak lines between 1500 - 1700 Å. The strongest lines all lie between 1350 Å and 1486 Å. As far as Fe VI is concerned, it has no transitions at wavelengths greater than 1500 Å, with all the strong ones having wavelengths shortward of 1380 Å. It is also worth noting the Fe V has the same ionization potential as N IV, thus making its existence in the WN4 - 6 winds very reasonable.

In Table 4 we have listed approximate wavelength positions of all emission features visible on the calcomp plots in our observations along with suggested identifications. With respect to the possible presence of Fe V and Fe IV, we can only state that at every wavelength position corresponding to strong Fe V lines, there is an emission feature in our spectra. The low resolution is not altogether the limiting factor for appropriate line identifications, since the large intrinsic width of WR emission lines results in severe line blending. As shown from high-dispersion optical spectra (Bappu 1973), several identifications are usually possible for a given line. In our case, Si III and Si IV have emission lines coincident with most of the Fe V and Fe VI lines. The exceptions are the lines at 1320 $\overset{o}{A}$, 1330 $\overset{o}{A}$, and 1586 $\overset{o}{A}$, where Fe V and Fe VI appear to be the only reasonable contributors, according to the line lists we searched.

Lines of Fe V have been identified in the spectra of the binary UW CMa (Drechsel et al. 1981), two WR's (Fitzpatrick 1982), and an O-type subdwarf (Bruhweiler 1981), although in the latter three objects they are presumably photospheric absorptions.

In conclusion, we attribute the apparent continuum variations shortward of 1550 $\overset{o}{A}$ in our IUE images to line variations, as observed in N IV 1718, with the major contributors being Fe V and possibility Fe VI. All lines having adequately populated lower

TABLE 4· Suggested Line Identifications

λ (Å)				
1243				N V 1243
1287		Si IV 1286		Fe VI 1285-88
1311	Si III 1312			Fe VI 1308,10
1320			Fe V 1318-23	
1330			Fe V 1330	Fe VI 1329-31
1340	Si III 1341-43		Fe V 1346	Fe VI 1338
1364	Si III 1362-65		Fe V 1361-66	Fe VI 1362
1377	Si III 1373	O V 1371	Fe V 1373-76	Fe IV 1371-75
1395		Si IV 1394	Fe V 1398	
1407		O IV 1407	Fe V 1407-09	
1420	Si III 1417		Fe V 1418-20	
1431	Si III 1433		Fe V 1430	
1440	Si III 1442		Fe V 1440-42	
1445	Si III 1447		Fe V 1447-49	
1470	O III 1477	Fe IV 1473	Fe V 1465-79	
1486		N IV 1486		
1505	Si III 1500-06			O V 1507
1532		Fe IV 1530-34		
1553		C IV 1548-51		N V 1549
1575		Fe IV 1577-78		
1586				Fe IV 1583
1625		Si IV 1624	Fe V 1623-27	N V 1620
1682		N IV 1687		
1705		Fe IV 1705		O V 1708
1721		N IV 1718		
1732	N III 1730			

levels can partake in the absorption of the O-star's continuum at relevant orbital phases, but only Fe V and Fe VI have the sufficient number of lines to generate a pseudo-continuum.

Radial Velocity Curves

One consequence of the selective atmospheric eclipses is the alteration of radial velocity curves. In Figure 7 we have plotted as a function of orbital phase the positions of maximum emission (V_E) and deepest absorption (V_A) for V444 Cyg, HD 90657, HD 186943, and HD 211853. The mean velocity for each system has been subtracted in each case.

In both 7(a) and 7(b), minimum velocity occurs at $\phi \sim 0.75$, as it should for a true radial velocity curve, since this is when the WR is approaching the observer and its lines have the maximum shortward shift. At $\phi \sim 0.25$, the velocity should be maximum. However, although the absorption component in Figure 7(b) does describe a somewhat typical RV curve, the emission component definitely does not. In fact, it has a maximum at $\phi \sim 0$, in addition to its amplitude being larger by about 50%. This is an example of the well-known problems besieging RV curves in WR stars; namely, for a given binary system, the RV curves derived from different emission lines have phase shifts, they have different amplitudes and zero-velocity values, and sometimes are distorted so
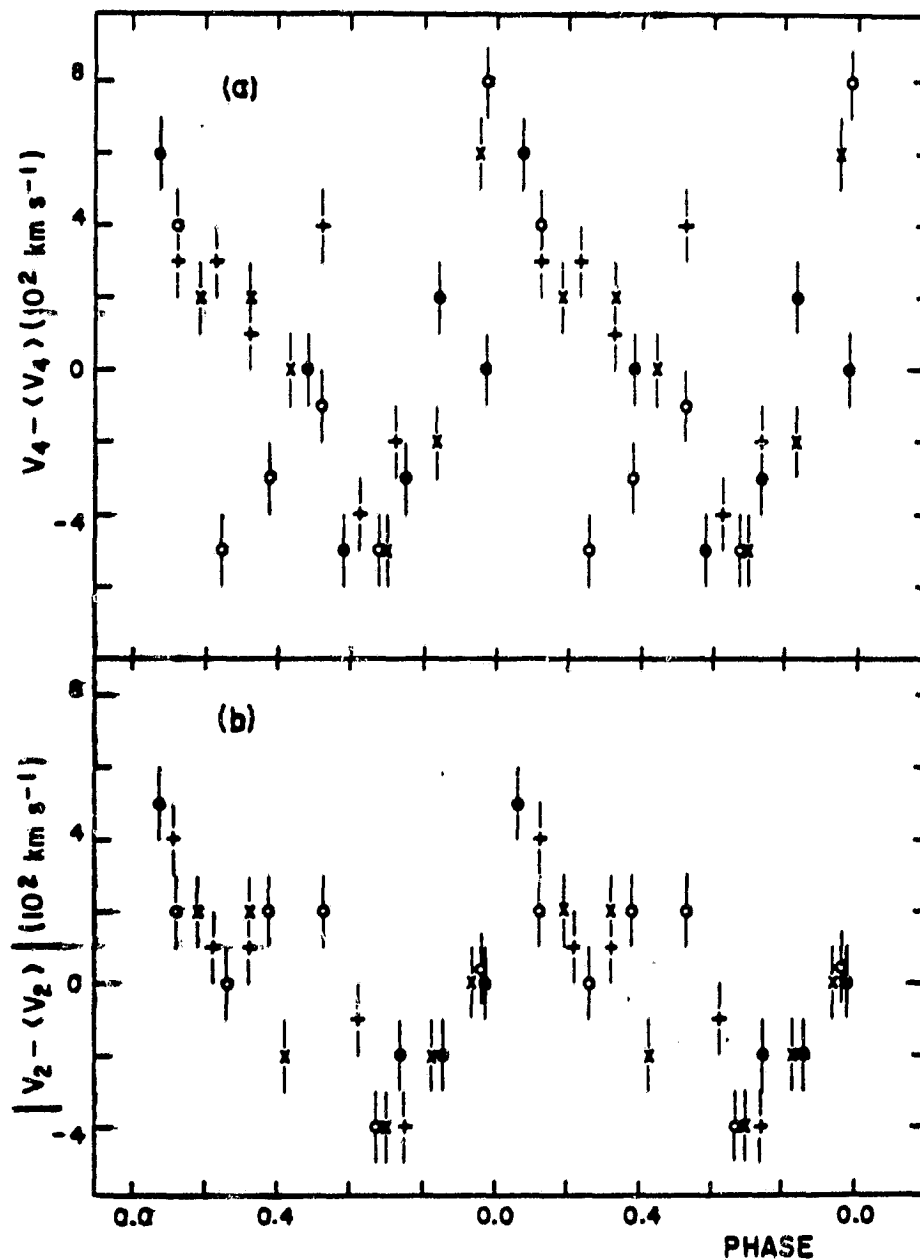
FIGURE 7: Position of emission mixima (a) and absorption minima (b)
in the N IV 1718 P Cygni line as a function of orbital phase.
Different symbols represent the same targets as in Figure 4.
Error bars correspond to the measurement uncertainties.

as to suggest non-circular orbits. This may now be understood in terms of the atmospheric eclipse interpretation.

At $\phi \sim 0$, the WR wind is absorbing the O-star's radiation. Since the latter is behind the WR wind, absorption will occur both shortward and longward of line center. However, due to wind-wind interaction effects the strongest absorption will occur shortward of line center. This will drive the centroid of the emission component to longer wavelengths at $\phi \sim 0$, as we see in Figure 7, distorting it. At the opposite phase, the absence of the shortward-shifted absorption will restore the emission line to its rest wavelength. The net result is a phase shift with respect to the true RV curve. The degree to which this effect is important depends upon the orbital inclination of the system, its separation, and the relative luminosity of the OB component. With respect to a given system, lines which show phase-dependent profile variations will most likely produce modified RV curves. Thus, for the determination of orbital parameters, it is best to choose emission lines that do not generally have a shortward-shifted absorption, whose zero-velocity best matches that of the OB component, and whose RV curve best resembles a true RV curve. These are the criteria generally applied, when possible.

Chapter III

EMPIRICAL OPTICAL DEPTH DISTRIBUTION

In Chapter I we pointed out that the observed emission line profiles in WR stars can be fit by model profiles with dissimilar combinations of source function and optical depth distributions (Castor 1970a). Thus, the wind structures cannot be unambiguously derived through theoretical model fitting alone. Therefore, an empirical determination of the optical depth distribution would be very useful in constraining the free parameters in the model calculations.

The optical depth along the line-of-sight to the O-star at the wavelength corresponding to the minimum in the N IV 1718 absorption (i.e., V_A) can be defined as

$$\tau_2 = -\ln \left(\frac{F_C(\phi)}{F_A(\phi)} \right) - 0.2$$

where $F_A(\phi)$ is the measured flux at orbital phases $0.75 < \phi < 1.25$ and $F_C(\phi)$ is the corresponding measured continuum flux. The factor 0.2 is substracted to account for the contribution to the absorption at V_A resulting from the projection of the WR wind onto the WR core. This value is taken from measurements of F_A/F_C in HD 193077 and HD 94546 and at orbital phases ~0.7 in HD 186943, which is the widest of our close WN + OB binary systems.

We will derive the dependence of optical depth upon impact parameter, p, which is related to the orbital phase by

$$p = a \left[\sin^2 (2\pi\phi) + \cos^2 (2\pi\phi) \cos^2 i\right]^{\frac{1}{2}}$$

where a is the orbital separation, and i is the inclination of the orbital plane.

Figure 8(a) is a plot of τ_2 as a function of impact parameter for values listed in Table 5. Different symbols correspond to different binaries, as in earlier figures. Note that by combining results from different systems in this manner we are assuming that the wind structures in WN4-6 stars are basically the same. The curve shown in this figure corresponds to a least-mean-squares fit to the data, resulting in

$$\tau_2 \propto p^{-1.1}$$

Before drawing any conclusions, the following cautionary remarks may be made. First, the material responsible for the absorption at V_A has a net outward (toward the observer) velocity. Thus, it has coordinates (p,z,) with $z > 0$ (see Figure 3). We have no means of determining z. Therefore, the dependence of τ_2 on p can only be regarded as an approximation to the true $\tau(r)$

FIGURE 8: (a) Optical depth distribution as measured from the minimum
flux level in the N IV 1718 absorption component as a
function of impact parameter. A least-mean square fit to
the data at $p > 14$ R_o is illustrated.

(b) Optical depth distribution as measured at λ_o, the
rest wavelength of the N IV 1718 transition in the WR
frame. A power law of the form $\tau_o \propto p^{-1}$ is superposed.
Propagated uncertainties for τ_o values are $\Delta\tau_o = \pm 0.4$
(see page 65).
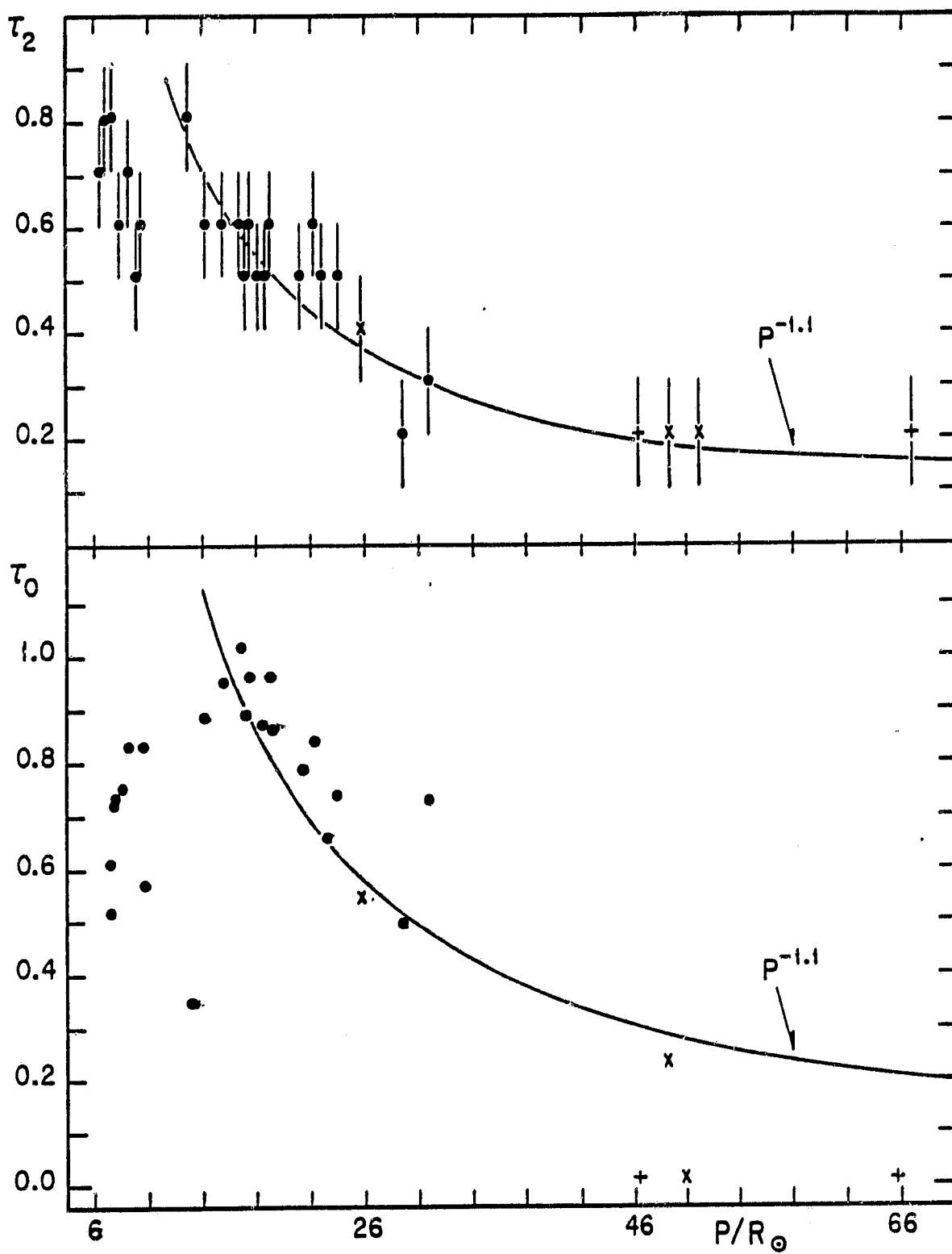
TABLE 5: Impact Parameters and Computed Optical Depths.

SWP	PHASE	$p(R_\odot)$	τ_2	τ_o
V444 Cyg				
13832	0.917	19.0	0.51	0.95
15380	0.852	29.0	0.17	0.48
15387	0.992	7.6	0.77	0.71
15388	0.998	7.4	0.72	0.60
15389	0.003	7.5	0.77	0.51
15390	0.008	7.6	0.77	0.72
15391	0.015	8.1	0.62	0.74
15392	0.020	8.6	0.72	0.82
15394	0.030	9.9	0.62	0.56
15396	0.051	13.5	0.77	0.34
15397	0.056	14.2	0.64	0.87
15399	0.066	15.9	0.64	0.94
15400	0.071	16.8	0.60	1.01
15401	0.076	17.7	0.62	0.95
15402	0.081	18.6	0.53	0.86
15403	0.085	19.3	0.64	0.78
15406	0.103	22.4	0.56	0.83
15407	0.108	23.2	0.53	0.65
15408	0.114	24.1	0.47	0.73

TABLE 5: Impact Parameters and Computed Optical Depths (continued)

SWP	PHASE	$p(R_\oplus)$	τ_2	τ_o
15588	0.835	31.0	0.29	0.72
15602	0.073	17.2	0.53	0.88
15644	0.974	9.4	0.49	0.84
HD 90657				
15584	0.83	49	0.19	0.23
15598	0.95	26	0.40	0.54
15618	0.19	51	0.11	0.0
HD 186943				
15578	0.11	47	0.2	0.0
15586	0.22	67	0.2	0.0

distribution. The accuracy of the approximation depends upon z being small enough to justify writing $r^2 = p^2 + z^2 \approx p^2$. Second, at small impact parameters the finite dimensions of the stellar cores become important, and they have been neglected. Third, the assumption of similarity between winds in WN4-6 stars may be questionable, and the points at $p > 30$ $R_\odot$ correspond to the two WN4 stars, while those a $p < 30$ $R_\odot$ belong to the WN5.

An optical depth distribution of the type $\tau \propto r^{-1.1}$ is consistent with a constant wind velocity distribution. That is, for a constant $v(r) = V_W$, conservation of mass flow in ($\dot{M} \propto r^2 \rho v$) demands $\rho \propto r^{-2}$, which if we assume that the populations of the levels go as the total density, implies that

$$\tau_2 \propto \frac{1}{r^2} \left(\frac{1}{r} - \frac{z^2}{r^3} \right)^{-1} \sim p^{-1}$$

where we have used equations 1 and 2 with the assumption of $z < p$. Thus, with previously stated reservations, we conclude that, to a first approximation, the velocity distribution in the winds of early WN stars is constant, at least beweeen ~14 and 66 $R_\odot$. Cherepashchuk, Eaton and Khaliullin (1981) concluded that the velocity is constant at $r > 12$ $R_\odot$ from their analysis of the optical eclipse light curves. Thus, the consistency of our results with previous observations is encouraging.

It is interesting to note that $\tau_2 > 0$ for impact parameters as large as 66 $R_\odot$, which means that the N IV ionization stage exists at least out to this distance from the WR core. Castor and van Blerkom (1970) found that the He II emitting region in the WN6 star HD 192163 extends out to 70 $R_\odot$. Assuming that this result is applicable to our WN4-6 stars, we are led to conclude that ions with different ionization potentials do indeed coexist in WN winds, as concluded by Willis (1982).

We will now describe an intuitively attractive method by which the measured optical depth can be associated with an exact position in the wind, thereby deriving the true optical depth distribution as a function of radius.

Consider the rest wavelength (λ_o) of a P Cyg feature such as N IV 1718, and consider an orbital phase $0.8 \lesssim \phi \lesssim 1.2$; i.e., when the O-star is behind a portion of the WR wind ($z < 0$ in Figure 3). Regardless of the velocity distribution in the WR wind, the only contribution to the absorption at the rest wavelength will come from material flowing perpendicular to the line-of-sight to the O-star. This material is situated at a distance $r \approx p$ from the WR core, and at $z = 0 \pm \frac{1}{2}z_{th}$, where z_{th} is the thermal length; i.e., the distance over which V_z changes by v_{th}, the thermal velocity of the particles at that point. V_z is the z-component of the expansion velocity. That is, a photon with wavelength λ_o

can be absorbed only by material traveling with a relative velocity (with respect to the source) $v < v_{th}$. Since in an expanding atmosphere τ_o counts only the absorbers in a narrow cross-section of the column along the line of sight (according to the Sobolev Theory), it can be expressed as

$$\tau_o = \int_{-z_{th/2}}^{z_{th/2}} \kappa \rho_i(r) dz$$

where ρ_i is the effective density of absorbing ions, and κ is the cross section for the transition.

A thermal path length z_{th} can be derived in the following manner:

$$V_z(r) = v(r) \cdot \frac{z}{(p^2 + z^2)^{\frac{1}{2}}} \approx v_{th}, \quad z = z_{th}$$

since $V_z(p,0) = 0$. Solving for z we find

$$z = z_{th} = \frac{p\, v_{th}}{v(r)} \cdot \frac{1}{\left(1 - v_{th}^2/v^2(r)\right)^{\frac{1}{2}}}$$

For typical WR winds, $v(r) \gg 300$ Km s^{-1} and $v_{th} < 30$ Km s^{-1} ($T_e \leq 50,000$ K). Therefore, $\left(v_{th}/v(r)\right)^2 \ll 1$, and

$$z_{th} \sim \frac{p\, v_{th}}{v(r)} = \frac{p\, v_{th}}{v(p)}$$

since $z \approx 0$, and $r \approx p$.

Hence, the optical depth at the rest wavelength of an emission line can be expressed as

$$\tau_0 = \kappa \rho_i(p)\, \frac{p v_{th}}{v(p)} \qquad \ldots\ldots 3$$

where

$$\kappa \rho_i(p) = \chi(p) = \frac{\pi e^2}{mc}\, (gf\lambda) \left[\frac{N_1}{g_1} - \frac{N_u}{g_u}\right] \frac{1}{v_{th}}$$

(Mihalas, p. 479). Equation 3 could also have been obtained directly from eqs. 1 and 2 by setting $z = 0$.

The density of absorbing ions is related to the total density
by

$$\rho_i(p) = f_i(p)\, \rho(p) \qquad \dots\dots 4$$

In addition, velocity and density are related by the conversation
of mass flow.

$$\dot{M} = 4\pi\, p^2\, \rho(p)\, v(p) \qquad \dots\dots 5$$

Combining 3, 4, and 5 and solving for v(p) we obtain

$$v(p) = \left(\frac{\kappa \dot{M} v_{th}}{4\pi}\right)^{\frac{1}{2}} \left(\frac{f_i(p)}{p\tau_o}\right)^{\frac{1}{2}} \qquad \dots\dots 6$$

If the density of absorbing ions followed the total density
distribution, $f_i(p)$ would be constant, and the above equation
could be used directly to derive v(r) by measuring τ_o. The impact
parameter p is presumably known. However, we cannot guarantee that
$f_i(p)$ = constant, which would mean that the ionization and
excitation levels are frozen in the wind. As mentioned previously,
there is evidence for a frozen ionization structure in WN winds,
but not for a frozen excitation structure (Willis 1982).

For illustrative purposes, we will now proceed to apply the method we have just described to our IUE observation, though any results that may be derived can only be regarded as tentative, due to the low resolution of the data.

We wish to determine the opacity of λ_o due to the bound bound transition $2s2p{}^1P - 2p^2\,{}^1D$ in N IV resulting from the absorption by ions in the WN wind of the O-star's continuum. By definition, radiation which emerges from an absorbing medium is expressed as

$$F = F_o\, e^{-\tau}$$

where F_o is the incident radiation. In this case, F_o corresponds to the continuum of the O-star. Given the errors which will be introduced by the low resolution of our observations, we are justified in assuming that the O-star continuum dominates the UV continuous energy distribution and that the measurable continuum level is generated primarily by the O-star. This is not a bad assumption since optical light curves of V444 Cyg suggest that the UV luminosity ratio is 5:1, with the O-star being the brighter. Hence, we adopt $F_o = F_c$, where F_c is the measurable continuum level.

As long as the O-star is far enough away from the material

flowing along the p axis, the interaction effects should not perturb

the material emitting at λ_c. Thus, we assume that the emission

at λ_o is constant throughout the orbital phases we will consider.

That is, we assume that the WR wind is stable, and that all alter-

ations of the profiles are due to underlying absorption.

At orbital phases $\phi \sim 0.5$, the flux we measure at λ_o can be

approximated by

$$F_m (\lambda_o, 0.5) = F_c(0.5) + F_e (\lambda_o) \qquad \ldots\ldots 7.$$

since the interaction effects should alter the profile mostly

in the shortwardmost regions. When the O-star is behind a part

of the wind at phase ϕ, the flux we measure is

$$F_m (\lambda_o, \phi) = F_c (\phi) e^{-\tau_o} + F_e (\lambda_o) \qquad \ldots\ldots 8$$

where $F_c (\phi) = F_c (0.5) e^{-\tau_c}$ and τ_c takes into account any

continuum opacity sources (such as electron scattering). We will

take $F_c (\phi)$ to be the measured continuum level at orbital phase ϕ,

at the 1718 $\overset{o}{A}$ region.

Combining equations 7 and 8 and solving for τ_0 we obtain

$$\tau_\sigma = -\ln\left[\frac{F_m\,(\lambda_o,\,\phi)\ +\ F_c\,(0.5)\ -\ F_m\,(\lambda_o,\,0.5)}{F_c(\phi)}\right]$$

The values of F_m were interpolated from a least mean squares fit to five points on the profile, centered on the rest wavelength of N IV 1718.5 in the WR's reference frame. The current IUE data extraction procedures permit flux values to be obtained at 1.2 $\overset{o}{A}$ intervals. Thus, 5 points represent one resolution element. All profiles were inspected visually to verify the interpolation. The F_c values were obtained by visual interpolation across the P Cyg feature, with the RDAF routine FEATURES.

Figure 8(b) is a plot of τ_0 as a function of impact parameter for the same spectra represented in Figure 8(a). The propagated uncertainties in this case are very large ($\Delta\tau_0 \approx 0.4$) and are not plotted. Despite this, we may venture a few comments. First, there is again a decrease in optical depth for $r < 14\ R_\odot$ as in Figure 8(a), while the data at larger radii can be represented by a power law of the form $\tau_0 \propto r^{-1.1}$. Second, the rapid decrease in optical depth at small distances from the core is reminiscent of the optical depth distributions employed by Castor (1970a) to produce realistic model profiles. Castor suggests that different

excitation conditions may prevail close to the WR core, as appears
to be the case according to Figures 8(a) and 8(b).

Equation 6 can be used to study the excitation structure of
the wind, once the velocity distribution is derived. When investi-
gating a given binary system, the ratio

$$\frac{f_i(p)}{f_i(p_f)} \frac{v^2(p_f)}{v^2(p)} = \frac{\tau(p)}{\tau(p_f)} \frac{p}{p_f}$$

can be constructed, thus eliminating the constants, and obtaining the
density of absorbing ions relative to that at p_f. In our case, we
have fixed $p_f = 31$ $R_\odot$ and plotted the points corresponding to
$f_i(p)/f_i(31)$ in Figure 9. We are adopting the result of the τ_2
analysis; i.e., $v(r) =$ constant and using only V444 Cyg data. This
figure seems to imply that the population of the lower level of the
N IV 1718 transition at $r = 7 - 10$ $R_\odot$ is a factor of two smaller
than at $r \sim 14$ $R_\odot$. Thus we may speculate that the population of the
lower level of the N IV 1718 transition increases with distance from
the WR core.

Willis (1982) has established a correlation between the
excitation potential (EP) of the lower level of a transition and
the velocity of the deepest portion of the absorption (V_A, in our
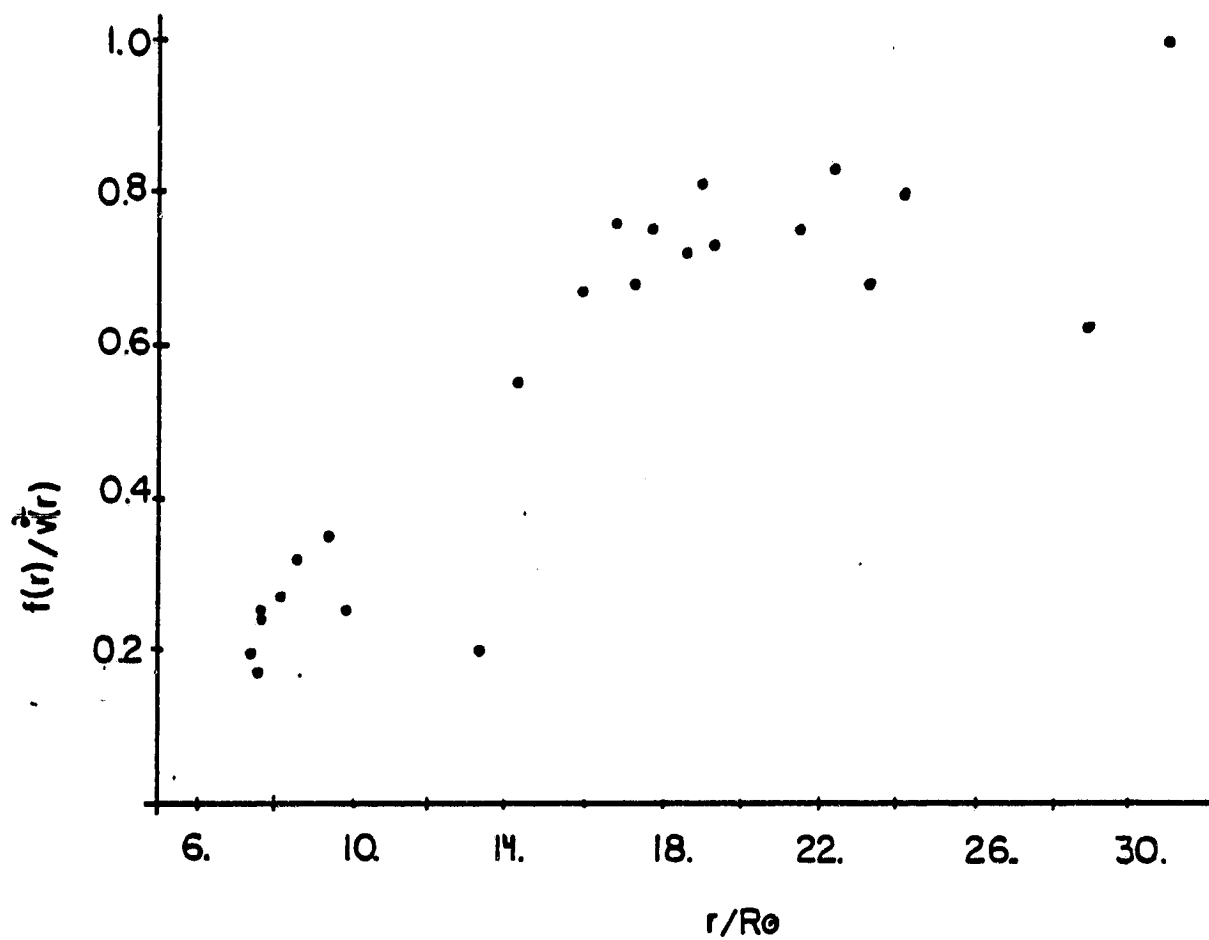notation). He finds that for a given star, V_A increases for lines

FIGURE 9: Possible dependence of the population of the N IV 1718 lower level on distance from the WR core, suggesting a changing excitation structure as a function of distance.

with lower EP. Thus, if one assumes an accelerating flow, excitation conditions decrease in the wind with increasing distance. According to our results, and those of Cherepashchuk, Eaton and Khaliullin (1980), the accelerating region must lie close to the WR core. The increasing optical depth between $r \sim 7$ and $r \sim 16$ $R_\odot$ in Figure 8(b) is in agreement with Willis' velocity - EP correlation since the EP of the N IV 1718 lower level is small (16.5 eV). That is, decreasing excitation conditions in the wind translate into increasing populations of low-lying levels.

We conclude by stressing that, due to the limitations of our data, the last remarks may only be regarded as speculative at this time.

Chapter IV

CONCLUSIONS AND RECOMMENDATIONS

The objectives of this investigation have been to analyze the variability of Wolf-Rayet binaries (WN + OB) in the ultraviolet spectral region $\lambda\lambda$ 1200 -1900 $\overset{o}{A}$, and determine whether the periodic, phase-dependent variations can be used to empirically derive the physical properties of the WN winds. We have found the variations in the UV to be similar in nature to those observed in the optical spectra. That is, there is a strengthening of absorption components in P Cygni-type features at orbital phases in which the O-star is behind the WR wind. With the aid of a computer code which models this type of variations, the dominant mechanism producing the variations is shown to be selective atmospheric eclipses of the OB component by the WR wind. Based on this explanation, a straightforward technique is proposed as a first step in determing the wind structure. The analysis of IUE observations applying this technique results in an empirical determination of an optical depth distribution in the WN winds which implies that a constant velocity law prevails at distances of 16 < r < 66 $R_\odot$. In addition, it suggest that the N IV ionization stage exist at least out to 66 $R_\odot$ consistent with the proposed constant ionization structure (Willis 1982). However, there may be an indication of a varying excitation structure at r < 16 $R_\odot$, which would be consistent with the observed velocity-excitation potential correlation which has been derived (Willis 1982).

The next steps that must be taken include: a) modeling the entire P Cygni profile using empirically determined parameters, b) applying the analyses to emission lines of different ionization and excitation potentials, and c) obtaining full phase coverage of additional sources.

As Castor (1970a) pointed out, WR profiles can be modeled and reproduced with a variety of dissimilar combinations of optical depth and source functions. We propose that the additional information required to restrict the free parameters in model profiles may be obtained from optical depth analyses similar to the ones we have performed. In particular, optical depth distributions such as those in Figure 7 can be used to fit model profiles to the observations.

Evidence supporting the existence of wind-wind collisions is provided by the variations in the C IV resonance line absorption component. Thus, an additional step that must be taken from the modeling standpoint is to include the wind-wind effects into the code. It is not clear at this point how one is to proceed on this question, unless the general solution to the problem of wind-wind collisions is derived. Furthermore, the interaction not only affects the OB star's wind; the structure of the WR wind must also be modified to a certain extent, and hence, a non-spherically symmetric wind velocity distribution would be more realistic for actual model profile fitting attempts.

Finally, it is important to repeat the analysis of Chapter III on additional emission lines having different ionization and excittation potentials. Excellent candidates are the lines of N V 4603, 4619, and N IV 3483. These undergo periodic variations of the same nature as N IV 1718 and may provide the additional information needed to separate the excitation and velocity structures.

REFERENCES

Abbot, D. C. 1982, Astrophys. J. 259, 282.

Ayres, T. R. 1982, Astrophys. J. 257, 243.

Bappu, M. K. V. 1973, in Wolf-Rayet and High Temperature Stars, IAU Symposium No. 49, M. K. V. Bappu and J. Sahade (eds.), D. Reidel Publishing Company, Dordrecht, p. 59.

Bappu, M. K. V. and Sahade, J. 1973, Wolf-Rayet and High Temperature Stars, IAU Symposium No. 49, D. Reidel Publishing Company.

Barlow, M. J., Smith, L. J., and Willis, A. J. 1981, Monthly Notices R. A. S. 196, 101.

Beals, C. S. 1929, Monthly Notices R. A. S. 90, 202.

Boggess, A. 1978a, Nature 275, 372.

Boggess, A. 1978b, Nature 275, 377.

Bruhweiler, F., Kondo, Y., and McCluskey, G. E. 1981, Astrophys. J. Suppl. Ser. 46, 255.

Cassinelli, J. P., Oloson, G. L., and Stalio R. 1978, Astrophys. J. 220, 573.

Castor, J. I. 1970a, Monthly Notices R. A. S. 149, 111.

Castor, J. I. 1970b, Astrophys. J. 160, 1187.

Castor, J. I. and van Blerkom, D. 1970, Astrophys. J. 161, 485.

Chapman, R. D. 1981, The Universe at Ultraviolet Wavelengths, NASA Conference Publication No. 2171.

Cherepashchuk, A. M. 1975, Soviet Astron. 19, 47.

Cherepashchuk, A. M. and Khaliullin, Kh. F. 1973, Soviet Astron. 17, 330.

Cherepashchuk, A. M., Eaton, Y. A., and Khaliullin, Kh. F. 1980, in Close Binary Stars. Observations and Interpretations, IAU Symposium No. 88, M. U. Plavec, D. M. Popper and R. K. Ulrich (eds.), D. Reidel Publishing Company, p. 193.

van der Hucht 1978, Ph.D. Thesis, Holland.

van der Hucht, K. A. 1979, Astron. Astrophys. Suupl. 38, 279.

Johnson, H. M. 1978, Astrophys. J. Suppl. Ser. 33, 83.

Khaliullin, Kh. F. and Cherepashchuk, A. M. 1975, Soviet Astron. 20, 186.

Kondo, Y., Meade, J. M., and Chapman, R. D. 1982, Advances in Ultraviolet Astronomy: Four Years of IUE Research, NASA Conference Publication 2238.

Kuhi, L. V. 1968, Astrophys. J. 152, 89.

Lamontagne, R., Moffat, A. F. J., Koenigsberger, G., and Seggewiss, W. 1982, Astrophys. J. 253, 230.

de Loore, C. W. H. 1982, in Wolf-Rayet Stars: Observations, Physics, Evolution, IAU Symposium No. 99, C. W. H. de Loore and A. J. Willis (eds.) D. Reidel Publishing Company, P. 343.

de Loore, C. and Willis, A. J. 1982, Wolf-Rayet Stars: Observations, Physics, Evolution, IUA Symposium No. 99, D. Reidel Publishing Company, Dordrecht.

Lucy, L. B. 1982, Astrophys. J. 255, 278.

Lucy, L. B. and White, R. 1980, Astrophys. J. 241, 300.

Massey, P. 1980, Astrophys. J. 244, 157.

Massey, P. 1981, Astrophys. J. 246, 153.

Massey, P. and Conti, P. S. 1980, Astrophys. J. 2

Massey, P. and Niemela, V. 1981, Astrophys. J. 245, 195.

Mihalas, D. 1978, Stellar Atmospheres, Second Edition, W. H. Freeman and Company, San Francisco.

Munch, G. 1950, Astrophys. J. 112, 266.

Niemela, V. and Moffat, A. F. J. 1982, Astrophys. J. 259, 213.

Nussbaumer, H., Schmutz, W., Smith. L. J., Willis, A. J., and Wilson, R. 1979, in The First Year of IUE, A. J. Willis (ed.), University College of London, p. 280.

Paczynski, B. 1973, in Wolf-Rayet and High Temperature Stars, IUA Symposium No. 49, M. K. V. Bappu and J. Sahade (eds), D. Reidel Publishing Company, Dordrecht p. 143.

Panek, R. 1981, IUE Newsletter No. 18, 68.

Prilutskii, O. F. and Usov, V. V. 1976, Soviet Astron. 20, 2.

Reader, J., Corliss, C. H., Wiese, W. L., and Martin, G. A. 1980, Wavelengths and Transition Probabilities for Atoms and Atomic Ions, U.S. Dept. of Commerce, NBS.

Sahade, J. 1958, Mem. de la Soc., Rayale Liege, Ser. IV, 20, 46.

Sanders, W. T., Cassinelli, J. P., and van der Hucht, K. A. 1982, in Wolf-Rayet Stars: Observations, Physics, Evolution, IAU Symposium No. 99, C. W. H. de Loore and A. J. Willis (eds.) D. Reidel Publishing Company, Dordrecht.

Sobolev, V. V. 1958, in Theoretical Astrophysics, V. Ambartsumain (ed.), Pergamon Press, London, Chapter 28.

Sobolev, V. V. 1960, The Moving Envelopes of Stars, Harvard University Press, Cambridge, Mass.

Sreenivasan S. R. and Wilson, W. J. F. 1982, Astrophys. J. 254, 287.

Thomas, R. N. 1973, in Wolf-Rayet and High Temperature Stars, IAU Symposium No. 49, M. K. V. Bappu and J. Sahade (eds.), D. Reidel Publishing Company, Dordrecht, p. 1.

Willis, A. J. 1982, Monthly Notices R. A. S. 198, 897.

Willis, A. J. and Wilson, R. 1978, Monthly Notices of the R. A. S. 182, 559.

Willis, A. J., Wilson, R., Macchetto, F., Beeckmanns, F., van der Hucht, K. A. and Stickland, D. J. 1979, in The First Year of IUE, A. J. Willis (ed.), University College, London.

Wilson, O. C. 1940, Astrophys. J. 91, 379.

APPENDIX

A computer code was constructed to model the phase-dependent profile variations in binary systems in which one member has a spherically expanding wind, or envelope. No interaction effects other than the absorption of radiation are taken into account. The treatment of the radiative transfer is based on the Sobolev Theory (1958,1960). Input parameters include the velocity and opacity distributions, which are assumed to be monotonic functions of distance. The source function is taken to be constant.

The profiles we will consider are composed of three parts.

a) a pure emission line arising in the spherically expanding wind, disregarding the presence of a continuum emitting core.

b) a shortward-shifted absorption component produced by the absorption in the wind of the continuum radiation emitted by the core (WR).

c) an absorption of the companion's continuum radiation by material in the WR wind at emission-line frequencies.

The emission (a) with the absorption (b) constitute a standard P Cygni profile, where the absorption component has a net shift to shorter wavelengths. This absorption arises in the column of wind material which is projected upon the central continuum-emitting core, and lies along the line of sight to the observer. In Figure 3, this

material is flowing along the +z axis, at p = 0. Clearly, for an expanding velocity field, the absorption can only occur at wavelengths shorter than λ_o, the wavelength of the transition in the rest frame of the central core. The depth of the absorption will depend upon the combination of opacity, velocity gradient along the line of sight, and intensity of the continuum source.

The only difference between the absorptions in (b) and (c) is that the latter can occur at $\lambda > \lambda_o$, since the secondary continuum source is behind a column of material expanding both away from it (i.e., toward the observer) and towards it.

It is worth noting that given our assumptions, the absorptions affect the emission line only insofar as they lower the underlying continuum level at selected frequencies. That is, the emission line retains its intrinsic profile and intensity, but the superposition of the absorptions produces an apparent decrease in emission intensity.

The free parameters in the model are:

RMAX   maximum extent of the emitting region. This is a useful parameter since it permits a cut-off in the emitting region before the density has fallen off considerably, which allows the possibility of a changing ionization structure.

VO,VN   specify the power law velocity distribution $v(r) =$ $VO\ r^{VN}$

CO,CN   specify the power law opacity distribution $CHI(r) =$ $CO\ r^{CN}$

PRIM,SEC   relative intensities of the WR and O-star's continua

RAD,VEL   orbital radius and veloctiy, respectively

WIDTH   total width of SEC's emission.

All distances are defined relative to the smallest radius of the WR emitting region, which may be taken as the WR core radius, R_c. Velocities are given in thermal units, and for convenience we have chosen $V_{th} = 10$ km s^{-1}. Intensities are in arbitrary units.

The large number of free parameters can be reduced to a great extent by adopting the results of Chapter III and using known orbital parameters. Hence, we may fix the following values:

VO = 150.   approximate terminal velocity 1500 km s^{-1}

VN = 0   constant velocity

CN = -2   assume $\rho_i(r) \propto \rho(r)$

VEL = 30.   typical orbital velocity = 300 km s^{-1}

WIDTH = 500.   secondary's (O-star) emission is continuum

RMAX = 70/R_c maximum extent of emission from FIG 8

RAD = 36/R_c orbital radius in V444 Cyg

We have devised a method to reduce the free parameters further, through a parametrization of the P Cygni profiles and a comparison with easily measurable quantities.

We define the following quantities:

$$\varepsilon = F_E/F_C$$
$$\alpha = F_A/F_C$$

where F_E, F_A, F_C are equivalent to the measured quantities in Table 2. If one chooses a velocity law, and specifies the inital opacity (CO), the code can be run for a grid of PRIM values. In the case of a single star, $F_C = $ PRIM, $F_E = F_E + $ PRIM, and $F_A = $ PRIM $(e^{-\tau})$. F_E is the maximum intensity of the pure computed emission. Using the resulting F_E, F_A, and F_C values, one can obtain (α,ε) points for every PRIM in the grid. When plotted (ε vs α), a smooth curve results. By choosing various values of CO, a family of curves is derived, as illustrated in Figure 10, where each curve is labeled with its corresponding CO value. It is important to note that the curves do not cross, so that a given point on the plot specifies the value of CO. The encircled "X" represents the (α,ε) point for the N IV 1718 line in HD 50896, and thus provides the value of CO to be used in model profile computations assuming a constant velocity distribution. It also provides the value of PRIM, since PRIM = $F_E/(\varepsilon-1)$. F_E is determined by the code once the opacity and velocity distributions are specified.
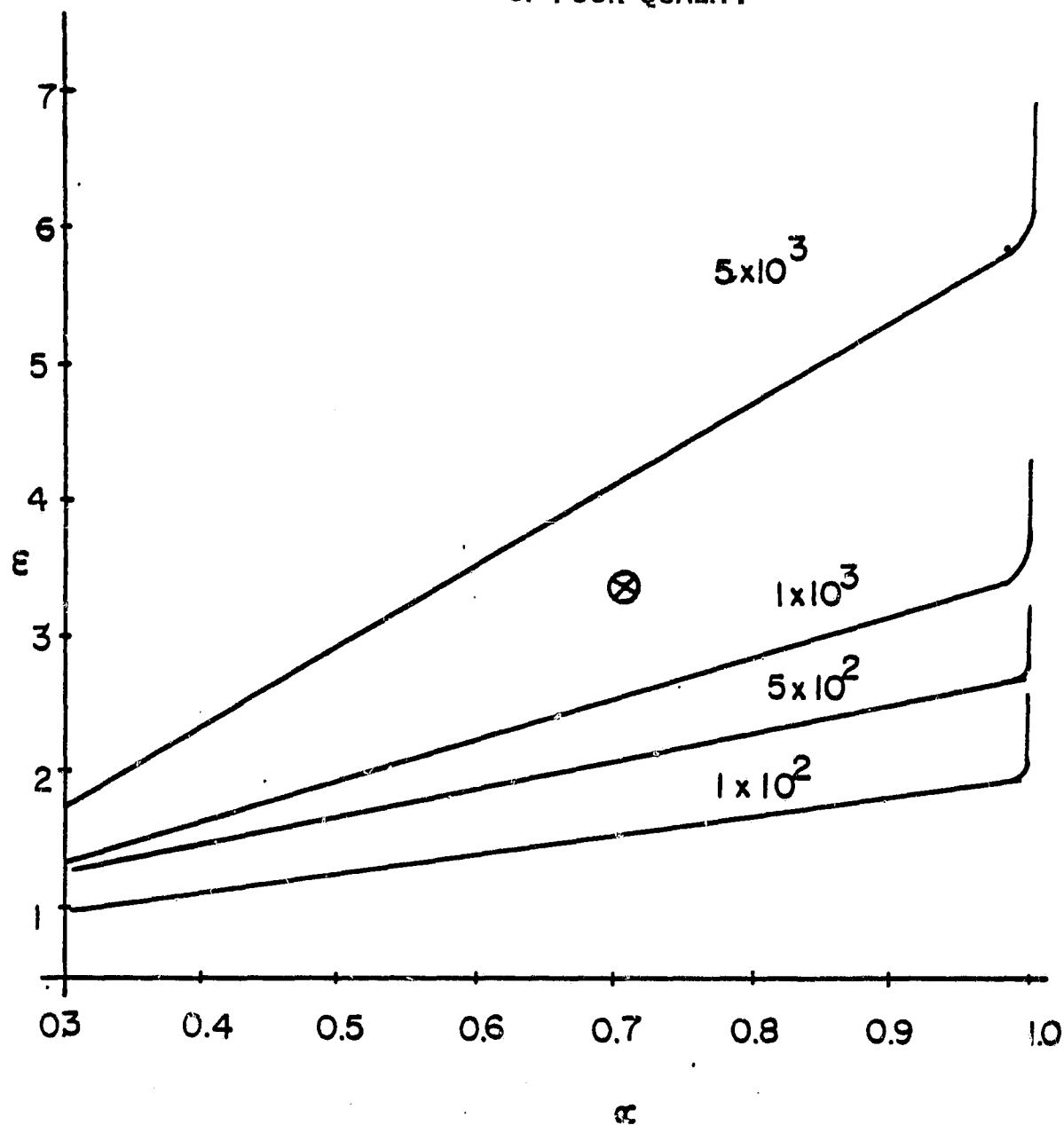
FIGURE 10: Model (α,ϵ) values for a single WE star as a function of
WR continuum intensity (PRIM) and initial opacity at the
surface of the core (CO) for a constant velocity law.
Curves are identified according to the CO value. The en-
circled "X" represents the N IV 1718 line in HD 50896.

Vita - Gloria Koenigsberger Avena

Born █████████ in ███████. Completed a "Licenciatura" in Physics at the Universidad Nacional Autonoma de Mexico in 1978 with a thesis entitled "Estrellas Wolf-Rayet: Variaciones Espectrales en HD 50896". Initiated Graduate studies with the Nassau Fellowship at Case Western Reserve University, Cleveland, Ohio, transferring to Penn State in 1980.

Job experience includes research and teaching assistantships at the UNAM from 1976 to 1979, Summer research assistantships at Kitt Peak National Observatory (1980), High Energy Astrophysics Lab in Goddard Space Flight Center, NASA (1981), and at Penn State with the X-ray Astronomy Group (1982). Associate Professor at the Institute of Astronomy of the UNAM, Mexico City, since March 1983.

Publications include:

1. Koenigsberger, G., Firmani, C. and Bissiachi, G. F. 1980, Rev. Mexicana Astron. Astron. Astrofis. 5, 45, "Spectral Variations in HD 192163".

2. Koenigsberger, G., Swank, J., Szymkowiak, A. and White, N. E. 1983, Astrophys. J. 268, 791, "X-Ray Properties of the Be/X-Ray System 2S0114 + 650 = LSI + 65 010".

Enjoys languages and is fluent in English, Spanish and French. Hobbies include: playing classical guitar and piano; sports such as jogging, horseback riding and swimming; stamp collecting; Ancient History; Mesoamerican archeology and archeoastronomy.